doxorubicin incorporated in liposomes in rats: I. Biopharm. Drug Dispos. 13, 155–170.

Herz, J., Gerard, R.D., 1993. Adenovirus-mediated transfer of low density lipoprotein receptor gene acutely accelerates cholesterol clearance in normal mice. Proc. Natl. Acad. Sci. U.S.A. 90, 2812–2816.

Huber, J.D., Egleton, R.D., Davis, T.P., 2001. Molecular physiology and pathophysiology of tight junctions in the blood-brain barrier. Trends Neurosci. 24, 719–725.

Huwyler, J., Wu, D., Pardridge, W.M., 1996. Brain drug delivery of small molecules using immunoliposomes. Proc. Natl. Acad. Sci. U.S.A. 93, 14164–14169.

Huwyler, J., Yang, J., Pardridge, W.M., 1997. Receptor mediated delivery of daunomycin using immunoliposomes: pharmacokinetics and tissue distribution in the rat. J. Pharmacol. Exp. Ther. 282, 1541–1546.

Ishida, O., Maruyama, K., Tanahashi, H., Iwatsuru, M., Sasaki, K., Eriguchi, M., Yanagie, H., 2001. Liposomes bearing polyethyleneglycol-coupled transferrin with intracellular targeting property to the solid tumors in vivo. Pharm. Res. 18, 1042–1048.

Klausner, R.D., Van Renswoude, J., Ashwell, G., Kempf, C., Schechter, A.N., Dean, A., Bridges, K.R., 1983. Receptor-mediated endocytosis of transferrin in K562 cells. J. Biol. Chem. 258, 4715–4724.

Klibanov, A.L., Maruyama, K., Beckerleg, A.M., Torchilin, V.P., Huang, L., 1991. Activity of amphipathic poly(ethylene glycol) 5000 to prolong the circulation time of liposomes depends on the liposome size and is unfavorable for immunoliposome binding to target. Biochim. Biophys. Acta 1062, 142–148.

Klibanov, A.L., Maruyama, K., Torchilin, V.P., Huang, L., 1990. Amphipathic polyethyleneglycols effectively prolong the circulation time of liposomes. FEBS Lett. 268, 235–237.

Lee, H.J., Boado, R.J., Braasch, D.A., Corey, D.R., Pardridge, W.M., 2002a. Imaging gene expression in the brain in vivo in a transgenic mouse model of Huntington's disease with an antisense radiopharmaceutical and drug-targeting technology. J. Nucl. Med. 43, 948–956.

Lee, H.J., Engelhardt, B., Lesley, J., Bickel, U., Pardridge, W.M., 2000. Targeting rat anti-mouse transferrin receptor monoclonal antibodies through blood-brain barrier in mouse. J. Pharmacol. Exp. Ther. 292, 1048–1052.

Lee, H.J., Zhang, Y., Zhu, C., Duff, K., Pardridge, W.M., 2002b. Imaging brain amyloid of Alzheimer disease in vivo in transgenic mice with an Abeta peptide radiopharmaceutical. J. Cereb. Blood Flow Metab. 22, 223–231.

Litzinger, D.C., Buiting, A.M., van Rooijen, N., Huang, L., 1994. Effect of liposome size on the circulation time and intraorgan distribution of amphipathic poly(ethylene glycol)-containing liposomes. Biochim. Biophys. Acta 1190, 99–107.

Liu, D., Mori, A., Huang, L., 1992. Role of liposome size and RES blockade in controlling biodistribution and tumor uptake of GM1-containing liposomes. Biochim. Biophys. Acta 1104, 95–101.

Maruyama, K., Ishida, O., Takizawa, T., Moribe, K., 1999. Possibility of active targeting to tumor tissues with liposomes. Adv. Drug Deliv. Rev. 40, 89–102.

Matlin, K.S., Reggio, H., Helenius, A., Simons, K., 1982. Pathway of vesicular stomatitis virus entry leading to infection. J. Mol. Biol. 156, 609–631.

Mori, A., Klibanov, A.L., Torchilin, V.P., Huang, L., 1991. Influence of the steric barrier activity of amphipathic poly(ethyleneglycol) and ganglioside GM1 on the circulation time of liposomes and on the target binding of immunoliposomes in vivo. FEBS Lett. 284, 263–266.

Omori, N., Maruyama, K., Jin, G., Li, F., Wang, S.J., Hamakawa, Y., Sato, K., Nagano, I., Shoji, M., Abe, K., 2003. Targeting of post-ischemic cerebral endothelium in rat by liposomes bearing polyethylene glycol-coupled transferrin. Neurol. Res. 25, 275–279.

Pardridge, W.M., 1999. Vector-mediated drug delivery to the brain. Adv. Drug Deliv. Rev. 36, 299–321.

Ponka, P., Lok, C.N., 1999. The transferrin receptor: role in health and disease. Int. J. Biochem. Cell. Biol. 31, 1111–1137.

Qian, Z.M., Li, H., Sun, H., Ho, K., 2002. Targeted drug delivery via the transferrin receptor-mediated endocytosis pathway. Pharmacol. Rev. 54, 561–587.

Rejman, J., Oberle, V., Zuhorn, I.S., Hoekstra, D., 2003. Size-dependent internalization of particles via the pathways of clathrin- and caveolae-mediated endocytosis. Biochem. J.

Schnyder, A., Krahenbuhl, S., Torok, M., Drewe, J., Huwyler, J., 2003. Targeting of skeletal muscle in vitro using biotinylated immunoliposomes. Biochem. J.

Shi, N., Boado, R.J., Pardridge, W.M., 2000. Antisense imaging of gene expression in the brain in vivo. Proc. Natl. Acad. Sci. U.S.A. 97, 14709–14714.

Shi, N., Boado, R.J., Pardridge, W.M., 2001. Receptor-mediated gene targeting to tissues in vivo following intravenous administration of pegylated immunoliposomes. Pharm. Res. 18, 1091–1095.

Shi, N., Pardridge, W.M., 2000. Noninvasive gene targeting to the brain. Proc. Natl. Acad. Sci. U.S.A. 97, 7567–7572.

Steven, A.C., Hainfeld, J.F., Wall, J.S., Steer, C.J., 1983. Mass distributions of coated vesicles isolated from liver and brain: analysis by scanning transmission electron microscopy. J. Cell. Biol. 97, 1714–1723.

Wolburg, H., Lippoldt, A., 2002. Tight junctions of the blood-brain barrier: development, composition and regulation. Vascul. Pharmacol. 38, 323–337.

Available online at www.sciencedirect.com
SCIENCE DIRECT®
Bioorganic & Medicinal Chemistry
ELSEVIER
Bioorganic & Medicinal Chemistry 13 (2005) 1811–1818

Synthesis and evaluation of *N*-(5-fluoro-2-phenoxyphenyl)-*N*-(2-[^{18}F]fluoromethoxy-d_2-5-methoxybenzyl)acetamide: a deuterium-substituted radioligand for peripheral benzodiazepine receptor

Ming-Rong Zhang,[a,b,*] Jun Maeda,[c] Takehito Ito,[a,b] Takashi Okauchi,[c] Masanao Ogawa,[a,b] Junko Noguchi,[a,b] Tetsuya Suhara,[c] Christer Halldin[d] and Kazutoshi Suzuki[a]

[a]*Department of Medical Imaging, National Institute of Radiological Sciences, 4-9-1 Anagawa, Inage-ku, Chiba 263-8555, Japan*
[b]*SHI Accelerator Service Co. Ltd, 5-9-11 Kitashinagawa, Shinagawa-ku, Tokyo 141-8686, Japan*
[c]*Brain Imaging Project, National Institute of Radiological Sciences, 4-9-1 Anagawa, Inage-ku, Chiba 263-8555, Japan*
[d]*Karolinska Institute, Department of Clinical Neuroscience, Psychiatry Section, Karolinska Hospital, S-17176 Stockholm, Sweden*

Received 6 October 2004; revised 24 November 2004; accepted 24 November 2004
Available online 22 December 2004

Abstract—*N*-(5-Fluoro-2-phenoxyphenyl)-*N*-(2-[^{18}F]fluoromethoxy-d_2-5-methoxybenzyl)acetamide ([^{18}F]**2**) is a potent ligand (IC_{50}: 1.71 nM) for peripheral benzodiazepine receptor (PBR). However, in vivo evaluation on rodents and primates showed that this ligand was unstable and rapidly metabolized to [^{18}F]F^- by defluorination of the [^{18}F]fluoromethyl moiety. In this study, we designed a deuterium-substituted analogue, *N*-(5-fluoro-2-phenoxyphenyl)-*N*-(2-[^{18}F]fluoromethoxy-d_2-5-methoxybenzyl)acetamide ([^{18}F]**5**) as a radioligand for PBR to reduce the in vivo metabolic rate of the non-deuterated [^{18}F]**2**. The design principle was based on the hypothesis that the deuterium substitution may reduce the rate of defluorination initiated by cleavage of the C–H bond without altering the binding affinity for PBR. The non-radioactive **5** was prepared by reacting diiodomethane-d_2 (CD_2I_2, **6**) with a phenol precursor **7**, followed by treatment with tetrabutylammonium fluoride. The ligand [^{18}F]**5** was synthesized by the alkylation of **7** with [^{18}F]fluoromethyl iodide-d_2 ([^{18}F]FCD_2I, [^{18}F]**9**). Compound **5** displayed a similar in vitro affinity to PBR (IC_{50}: 1.90 nM) with **2**. In vivo evaluation demonstrated that [^{18}F]**5** was metabolized by defluorination to [^{18}F]F^- as a main radioactive component, but its metabolic rate was slower than that of [^{18}F]**2** in the brain of mice. The deuterium substitution decreased the radioactivity level of [^{18}F]**5** in the bone of mouse, augmented by the percentage of specific binding to PBR in the rat brain determined by ex vivo autoradiography. However, the PET image of [^{18}F]**5** for monkey brain showed high radioactivity in the brain and skull, suggesting a possible species difference between rodents and primates.

1. Introduction

Peripheral benzodiazepine receptor (PBR) is located on the mitochondrial outer membrane in peripheral organs including the kidney, nasal epithelium, lung, heart, and endocrine organs such as the adrenal, testis, and pituitary gland, and in the central nervous system.[1,2] Since the PBR density was found to increase in injured brains and tumor regions, PBR imaging of PBR in these areas has become an attractive study target.[3–8] The putative relationship between PBR and brain diseases (Alzheimer's disease, Parkinson's disease, stroke, encephalitis etc.) or tumors (lung cancer, liver cancer, gastric cancer etc.) has promoted the development of a PET ligand, which could be used for visualizing the distribution and examining the change of PBR in these regions.[9–12]

We recently developed a PET ligand, [^{11}C]*N*-(2,5-dimethoxybenzyl)-*N*-(5-fluoro-2-phenoxyphenyl)acetamide ([^{11}C]DAA1106, [^{11}C]**1**, Scheme 1), for imaging PBR in the primate brain.[13,14] The in vitro and in vivo evaluation of mice, rats, and monkeys demonstrated that [^{11}C]**1** had high specific binding with PBR in the brains and had about a 4-fold higher uptake into the monkey brain than [^{11}C]PK 11195,[15,16] a commonly

Keywords: Peripheral benzodiazepine receptor; Deuterium substitution; Defluorination; PET.
*Corresponding author. Tel.: +81 43 206 4041; fax: +81 43 206 3261; e-mail: zhang@nirs.go.jp

0968-0896/$ - see front matter © 2004 Elsevier Ltd. All rights reserved.
doi:10.1016/j.bmc.2004.11.058

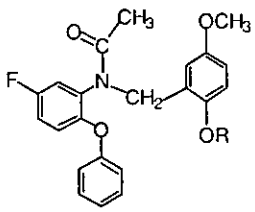

[^{11}C]DAA1106 ([^{11}C]1): R = $^{11}CH_3$
[^{18}F]FMDAA1106 ([^{18}F]2): R = $^{18}FCH_2$
[^{18}F]FEDAA1106 ([^{18}F]3): R = $^{18}FCH_2CH$

Scheme 1. Chemical structures of [^{11}C]DAA1106 ([^{11}C]1) analogues.

used PET ligand for imaging PBR in the primate brain. Now, [^{11}C]1 is being used to investigate PBR in the human brain in our facility.

Using [^{11}C]1 as a lead compound, we further synthesized and evaluated two novel [^{18}F]alkyl analogues [^{18}F]FMDAA1106 ([^{18}F]2) and [^{18}F]FEDAA1106 ([^{18}F]3) by replacing the positron emitter ^{11}C for ^{18}F (Scheme 1).[17,18] The fluoromethyl analogue 2 (IC_{50}: 1.71 nM) and fluoroethyl analogue 3 (0.77 nM) had similar or higher potency for PBR than 1 (1.62 nM). Ligand [^{18}F]3 had a similar property to [^{11}C]1 as a potent and specific PET ligand for PBR, and showed 1.5 times higher uptake into the monkey brain than [^{11}C]1. This promising results led to the clinical investigation of PBR using [^{18}F]3 to follow [^{11}C]1. In contrast, although [^{18}F]2 also passed through BBB and entered into the brain, this ligand exhibited a much higher uptake in monkey skulls, and it had at least 50 times higher radioactivity in the bones of mice than [^{18}F]3 at 120 min after injection. Metabolite analysis demonstrated that [^{18}F]2 was rapidly decomposed to [^{18}F]F^- in the plasma and brain of mice. The high accumulation of [^{18}F]F^- into the bone with a long residence time should decrease the effective signal and give a low sensitivity of PET image of the brain. Moreover, the presence of [^{18}F]F^- in the brain could interfere with the determination of 'real' specific binding of [^{18}F]2 to PBR, and augment non-specific binding in the examined regions.

It was demonstrated that defluorination of the fluoromethyl moiety was a main metabolic route of [^{18}F]2 as shown in Scheme 2.[18] The carbon–hydrogen (C–H) bond of the [^{18}F]fluoromethyl moiety may firstly be attacked by enzyme and cleaved, followed by the elimination of hydrofluoride from the same α carbon atom to generate a carbene structure (4). Carbene 4 was stabilized by resonating it with the adjacent oxygen atom, which further promoted the decomposition of [^{18}F]2. Thus, cleavage of the C–H bond is considered as a rate-limiting step, which contributes to the metabolism of [^{18}F]2.

In this study, we designed a deuterium-substituted analogue of [^{18}F]2, *N*-(5-fluoro-2-phenoxyphenyl)-*N*-(2-[^{18}F]fluoromethoxy-d_2-5-methoxybenzyl)acetamide ([^{18}F]5), as a novel radioligand for PBR (Scheme 2). The design principle was as follows: since the deuterium atom has a similar and bioisoteric property to the hydrogen atom, deuterium substitution may only have minimal influence on the potential affinity of 5 for PBR. On the other hand, the substitution can be expected to reduce the rate of defluorination of the [^{18}F]fluoromethyl moiety since carbon–deuterium (C–D) bond is generally stronger to break than the C–H bond. We firstly synthesized the non-radioactive 5 and its 18-fluorine labeled analogue [^{18}F]5 and measured the in vitro binding affinity of 5 for PBR. We then compared the metabolic rate of [^{18}F]5 with that of [^{18}F]2 in the plasma and brain of mouse, and examined the regional distribution of [^{18}F]5 in the mice, rats, and monkey.

2. Results and discussion

2.1. Chemistry

The non-radioactive fluoromethyl-d_2 analogue 5 was synthesized as shown in Scheme 3. The reaction of excess diiodomethane-d_2[17] (CD_2I_2, 6) with *N*-(5-fluoro-2-phenoxyphenyl)-*N*-(2-hydroxy-5-methoxybenzyl)acetamide[19] (7) in the presence of NaH at 25 °C gave iodomethyl-d_2 analogue 8 and a dimmer of 7 as a main

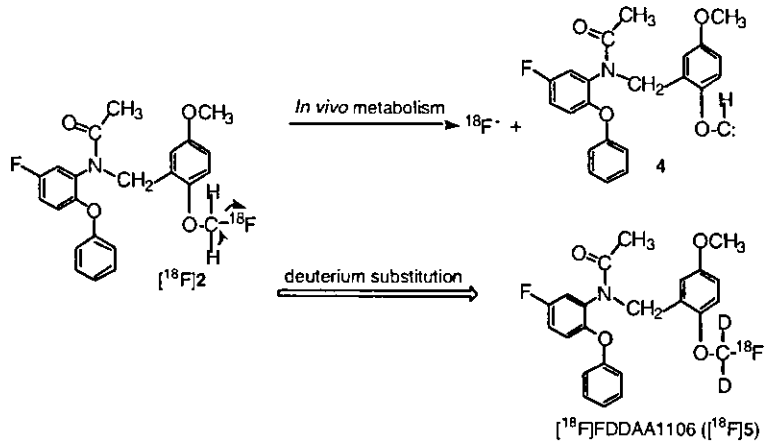

Scheme 2. In vivo metabolism of [^{18}F]2 and design of [^{18}F]5.

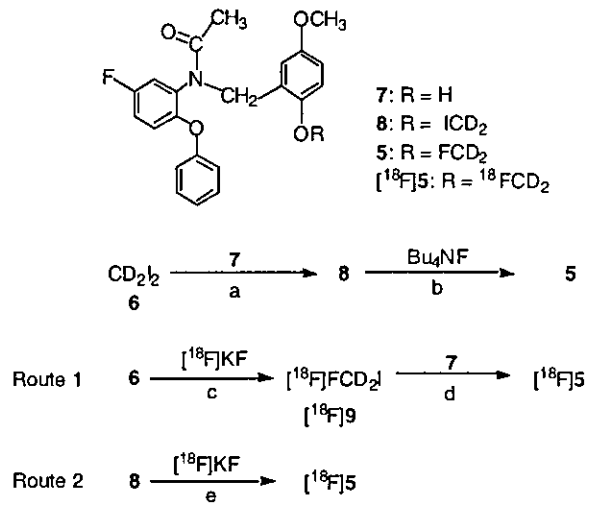

Scheme 3. Synthesis of 5 and [^{18}F]5: (a) NaH, DMF, 25 °C, 3 h, 15%; (b) THF, reflux, 8 h, 64%; (c) *o*-dichlorobenzene, 110 °C, 2 min, 23%; (d) NaH, DMF, −15 °C, 2 min, 92%; (d) DMF, 30–120 °C, 1–15 min, 0–35%.

by-product. The treatment of **8** with tetrabutylammonium fluoride afforded **5** at a total yield of 10% starting from **7**.

The radiosynthesis of [^{18}F]**5** was performed by two routes, respectively (Scheme 3). One route was a two-step reaction sequence, which involved the synthesis of the radioactive intermediate [^{18}F]fluoromethyl-d_2 iodide[20] ([^{18}F]FCD_2I, [^{18}F]**9**), followed by the alkylation of phenol precursor **7** with [^{18}F]**9**. Another route was the direct nucleophilic replacement of **8** with [^{18}F]F^-. In the two-step method, the intermediate [^{18}F]**9** was prepared by the fluorination of **6** with [^{18}F]F^- in the presence of K_2CO_3 and 4,7,13,16,21,24-hexaoxa-1,10-diazabicyclo[8,8,8]hexacosane (Kryptofix 222) as a phase-transfer agent by using an automated synthesis device.[21] The formed [^{18}F]**9** was distilled from the reaction mixture, passed through short columns filled with Ascarite and phosphorus pentoxide, and trapped in a DMF solution containing **7** and NaH at −15 °C. This procedure gave a pure and highly reactive [^{18}F]**9**, since the distillation could leave behind all non-volatile impurities such as metal ions from the cyclotron target, the unreacted [^{18}F]F^- and Kryptofix 222/K_2CO_3. After [^{18}F]**9** trapping was completed, the reaction of **7** with [^{18}F]**9** proceeded perfectly to form [^{18}F]**5**. In the direct method, heating **8** with [^{18}F]F^- at 30–120 °C could give [^{18}F]**5**, but the radiochemical yield was not reproducible (0–35%). Moreover, purifying the product from the reaction mixture was often complicated because excess Kryptofix/K_2CO_3 and the impurities resulting from the target significantly decreased the purification efficiency. Thus, [^{18}F]**5** was synthesized by the two-step reaction method via [^{18}F]**9** for animal experiments.

Semi-preparative HPLC purification on the reverse phase for the reaction mixture gave [^{18}F]**5** in 13 ± 6% (n = 4) radiochemical yield based on [^{18}F]F^-, corrected for the decay at the end of bombardment in a synthesis time of 50 ± 3 min. The identity of the desired product was confirmed by co-injection with the non-radioactive **5** using analytic HPLC. In the final product solution, the radiochemical purity of [^{18}F]**5** was higher than 98% with a specific activity of 40–70 GBq/μmol as determined from the mass measured by the HPLC/UV analysis. No significant peak corresponding to **7** or other impurities relative to **7** was observed in the HPLC chart for the final product. Moreover, the radiochemical purity of [^{18}F]**5** remained >95% after it was left at 25 °C for 180 min, and this product was stable as a PET ligand while performing animal experiments.

2.2. Evaluation

In a previous study, the rapid metabolism of fluoromethyl ligand [^{18}F]**2** by defluorination in the brain and plasma precluded its usefulness for the clinical investigation of PBR.[18] The high accumulation of [^{18}F]F^- in the bone including the skull with a long residence time could decrease the effective signal of PET imaging of [^{18}F]**2** in the brain and create difficulties on the data analysis. Furthermore, the presence of [^{18}F]F^- might augment the non-specific binding in the examined regions, and then interfere with the determination of the specific binding for PBR. It was found that [^{18}F]F^- was generated by in vivo defluorination, which might be initiated by cleavage of the C–H bond as a rate-limiting step. Therefore, to reduce the rate of defluorination starting from break of the C–H bond, we considered the usefulness of the isotopic effect of deuterium on hydrogen. Due to the lower zero-point energy (difference: 6–9 kJ/mol) and the lower vibration frequency (difference: 788 cm^{-1}) of the C–D bond than the C–H bond, the C–D bond is generally more difficult to break than the C–H bond.[22] It was reported that the cleaving rate of the C–H bond was about 6.7 times faster at 25 °C, and 3.3 times faster at 200 °C than that of C–D.[22] There were several examples of the deuterium-substituted PET ligands for MAO B[23] and 5-HT_{2A}[24] receptors improving the properties of the corresponding non-deuterated ligands by reducing their in vivo metabolic rates. In this study, we compared the in vitro binding affinity, metabolic rate and regional distribution of [^{18}F]**5** with those of the non-deuterated [^{18}F]**2**.

2.2.1. In vitro binding affinity for PBR and CBR. The in vitro binding affinities (IC_{50}) of **5** and **8** for PBR were measured from competition for the [^{11}C]**1** binding using quantitative autoradiography according to the procedures as described previously.[18,25] As shown in Table 1, **5** displayed a similar affinity than **2** for PBR, and this value was also little lower than that of **1** and about 4-fold higher than PK 11195. The iodomethyl-d_2 analogue **8** had about 27 times weaker affinity than **5**, suggesting that the relative bulk group contained in this series of derivatives was not favorable for expressing the binding potency of PBR. On the other hand, **5** and **8** displayed negligible affinities for central benzodiazepine receptor (CBR) measured by using CBR-selective [^{11}C]flumazenil. The high selectivity of PBR/CBR of the two analogues may be due to their structural difference from the typical benzodiazepine structure.[20] Although the

Table 1. In vitro binding affinity (IC_{50}) for PER and CBR, and octanol/phosphate buffer distribution coefficient (log *P*)

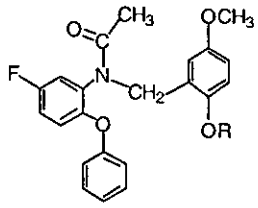

Ligand	R	IC_{50}(nM)[a]		log *P*[d]
		PBR[b]	CBR[c]	
5	FCD2	1.90	>10,000	3.76
8	ICD2	52.30	>10,000	4.26
2	FCH2	1.71	>10,000	3.70
1	CHS	1.62	>10,000	3.65
PK11195		8.26	>10,000	

[a] Values represent the mean obtained from nine concentrations of compound using at least eight slices of rat brain ($n = 3$).

[b] [^{1}C]DAA1106 was incubated in the presence of the compounds examined.

[c] [^{11}C]Flumazenil was incubated in the presence of the compounds examined.

[d] The log *P* values were determined in the phosphate buffer (pH = 7.4)/octanol system using the shaking flask method. All results were presented as mean values ($n = 3$) with a maximum range of ±5%.

deuterium atom is larger than hydrogen, the deuterium substitution does not alter the molecular similarity and bioisoteric property between the two functional groups of *O*-CD_2F and *O*-CH_2F. The difference between the two molecules is too small to have significant influence on their affinities for PBR.

2.2.2. Metabolism in the plasma and brain of mouse. The metabolite analysis of [^{18}F]**5** was performed in the brain and plasma of mice. After i.v. injection of [^{18}F]**5** (8 MBq) into mice ($n = 3$) at designated time points, the plasma and brain homogenate were obtained and immediately deproteinized with CH_3CN. Extraction of the radioactivity in the plasma and brain homogenate into CH_3CN was efficient, and the recovered yield was >70%. The radioactive metabolite of [^{18}F]**5** was identified using HPLC with a highly sensitive detector[26] for radioactivity. In all samples, a radioactive component was determined in addition to the unchanged [^{18}F]**5**. As estimated by its retention time ($t_R = 2.0$ min), this metabolite was much more polar than [^{18}F]**5** ($t_R = 10.2$ min). Moreover, the t_R of the peak remained unchanged when treated with a base or acid. Using ion exchange chromatography and TLC, this product was assigned to [^{18}F]F^-, which was identified by co-injecting and developing with non-radioactive standard KF solution. As it was improbable brain permeable, [^{18}F]F^- was produced in the plasma and brain, respectively. This result suggested that defluorination of the [^{18}F]fluoromethyl moiety was the main metabolic route of [^{18}F]**5**, and the deuterium substitution did not change its main metabolism route.

Figure 1 shows the percentages of unchanged [^{18}F]**5** and [^{18}F]**2** in the plasma and brain of mice measured by

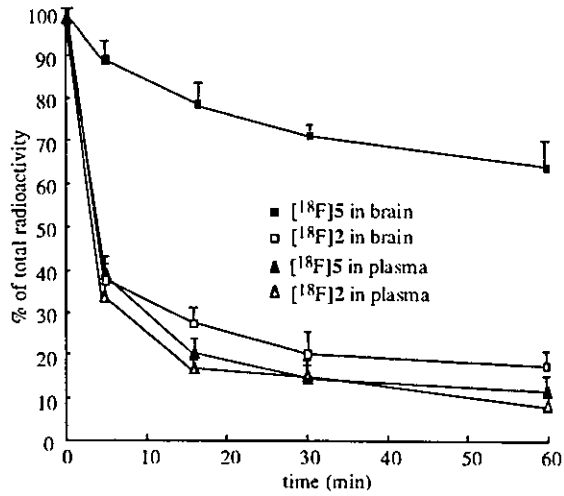

Figure 1. Percentage (mean ± s.d., $n = 3$) conversion of [^{18}F]**5** to metabolite in the mouse plasma and brain at several time points after i.v. injection of [^{18}F]**5** (5–10 MBq) into the mice. The unchanged [^{18}F]**5** and metabolite were analyzed by HPLC for CH_3CN extracts from the plasma and brain homogenate prepared as described in the experimental.

HPLC. We conducted two-way repeated ANOVA to compare the time courses of [^{18}F]**5** with those of [^{18}F]**2** in the brain and plasma, respectively. In the plasma, no significant interaction was determined between the two ligands. The half life ($T_{1/2}$) in the plasma was 2.575 min for [^{18}F]**5** and 2.367 min for [^{18}F]**2**. In the brain, a significant interaction ($F_{1/16} = 83{,}93$, $P < 0.01$) was determined between them. The half life ($T_{1/2}$) of [^{18}F]**5** in the brain was >60 min, whereas that of [^{18}F]**2** was only 2.227 min. The mechanism of the different metabolic rates between the two ligands in the brain was that the C–D bond of [^{18}F]**5** was more difficult to break by enzyme than the C–H bond of [^{18}F]**2**, which was the rate-limiting step contributory to their metabolism.

The difference of the metabolic rates of [^{18}F]**2** and [^{18}F]**5** in mouse brain was remarkable, compared with that in the mouse plasma. We considered that a same enzyme is related to their metabolism in the plasma and brain. In general, the level of enzyme metabolizing a parent ligand in plasma is much higher that in brain. Therefore, the different level of the same enzyme metabolizing [^{18}F]**2** and [^{18}F]**5** in the brain and plasma was a contributing factor for the difference of their metabolic rates. The level of enzyme attacking the C–H and C–D bonds in the plasma may be too high to distinguish difference of the two bonds, whereas that in the brain may be apt to realize the difference.

2.2.3. Regional distribution. The radioactivity distribution of [^{18}F]**5** in the mice was examined and compared to that of [^{18}F]**2** at 5–120 min after injection. Table 2 shows the decay-corrected percent dose per gram (% ID/g) data of [^{18}F]**2** and [^{18}F]**5** in the brain, blood and bone. The radioactivity level of [^{18}F]**5** in the bone was 1.6% ID/g at 120 min after injection, and was 30% of [^{18}F]**2** level in the bone. On consideration of the ten-

Table 2. Distribution (% injected dose/g tissue: mean ± s.d., $n = 3$) of [^{18}F]ligand in Mice at 5, 15, 30, 60, and 120 min after injection

Ligand	Tissue	5 min	15 min	30 min	60 min	120 min
[^{18}F]**2**	Blood	0.95 ± 0.09	1.34 ± 0.54	0.76 ± 0.32	0.54 ± 0.18	0.49 ± 0.18
	Brain	2.65 ± 0.85	3.26 ± 1.07	4.39 ± 1.38	4.04 ± 1.95	3.47 ± 0.94
	Bone	0.58 ± 0.23	1.98 ± 1.99	2.51 ± 1.35	3.91 ± 0.86	5.64 ± 0.72
[^{18}F]**5**	Blood	0.78 ± 0.23	0.92 ± 0.15	0.83 ± 0.20	0.86 ± 0.33	0.52 ± 0.15
	Brain	2.31 ± 0.92	2.93 ± 1.01	3.68 ± 1.43	3.62 ± 0.85	3.24 ± 0.70
	Bone	0.58 ± 0.29	0.74 ± 0.05	1.23 ± 0.08	1.59 ± 0.01	1.63 ± 0.04

dency of [^{18}F]F^- to readily accumulate in bone, the radioactivity examined in the bone was mostly due to [^{18}F]F^-. In contrast, [^{18}F]**2** and [^{18}F]**5** displayed a similar level of radioactivity in the brain and blood. The cause may be that the two ligands had similar affinity for PBR, lipophilicity and other physiochemical properties. Although they were metabolized in the brain in different rates after they entered into the brain, the main radioactive metabolite [^{18}F]F^- may be retained in the brain without a rapid clearance, which did not give significant difference for their total radioactivity levels in the brain.

Figure 2 shows ex vivo autoradiograms of rat brains at 30 min after injection of [^{18}F]**5**. As can be seen in the sagittal section of the control brain (Fig. 2a), [^{18}F]**5** showed a high uptake, consistent with the distribution data measured above (Table 2). High radioactivity levels were observed in the olfactory bulb and cerebellum, whereas low uptakes were seen in the other brain regions such as the frontal cortex and striatum. The uptake pattern of radioactivity was in accordance with the regional distribution of PBR in the brain and was similar to those of [^{11}C]**1** and [^{18}F]**3**.[14,17,27] Co-injection of [^{18}F]**5** with the non-radioactive **1** (1 mg/kg) produced a reduction of radioactivity in the brain regions having PBR (Fig. 2b). The radioactivity level in the olfactory bulb and cerebellum was decreased to 30–40% of the control, while the reduction ratio of [^{18}F]**2** by **1** was about 50%.[18] In spite of remarkable difference of the metabolic rate of the two ligands in the brain, the difference of their nonspecific bindings determined by ex vivo autoradiography was not so significant. From the metabolic route of [^{18}F]**2** and [^{18}F]**5**, we considered that the nonspecific binding of the two ligands was mainly due to [^{18}F]F^- in the brain. Although [^{18}F]F^- does not bind to the receptor, the [^{18}F]F^- might be partly retained in the olfactory bulb and cerebellum, and could not be released by the co-injection of **1**, which kept the nonspecific binding of [^{18}F]**2** and [^{18}F]**5** at a similar level. The left [^{18}F]F^- might spread around the brain and did not clear out from the brain rapidly, which led to a different distribution of [^{18}F]F^- in the whole brain. In fact, the ratio of olfactory bulb to frontal cortex was 2.1 ± 0.3 for [^{18}F]**5**, whereas the ratio for [^{18}F]**2** was only 1.6 ± 0.5 in the corresponding regions. This finding supported that the [^{18}F]F^- level was lower for [^{18}F]**5** than for [^{18}F]**2** in the whole brain including the frontal cortex.

Figure 3 shows a typical PET summation image of monkey brain acquired from 30 to 180 min after [^{18}F]**5** injection (80 MBq/1.5 mL). Unexpectedly, although a high radioactivity was observed in the monkey brain, the PET image of [^{18}F]**5** displayed much higher accumulation of radioactivity in skull. Moreover, the level of radioactivity of [^{18}F]**5** in the monkey skull was similar to that of [^{18}F]**2**[18] by comparing their PET images at a normalized injection dose. This image gave a visual evidence that [^{18}F]**5** was metabolized by in vivo defluorination to [^{18}F]F^-, which was accumulated into the bone.

In this study, the isotopic effect induced a distinct reduction in the metabolic rate of [^{18}F]**5** in the brain of mice

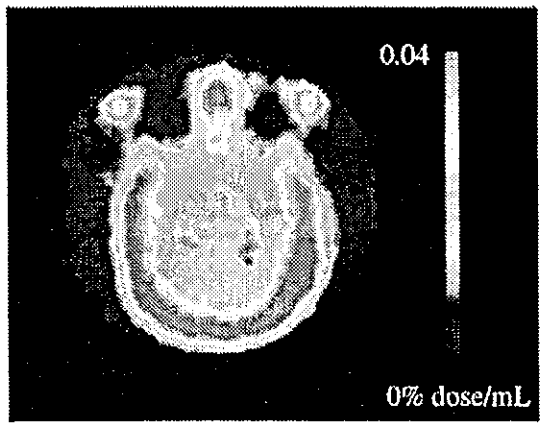

Figure 3. PET summation image of the monkey brain acquired between 30 and 180 min after [^{18}F]**5** injection (80 MBq).

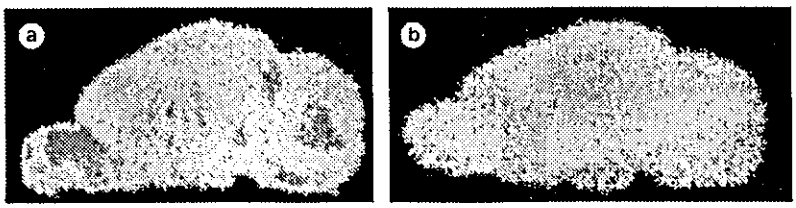

Figure 2. Ex vivo autoradiogram of [^{18}F]**5** in the sagittal sections of rat brains at 30 min after injection (20–25 MBq). (a) [^{18}F]**5**; (b) [^{18}F]**5**+**1** (1 mg/kg).

although the deuterium substitution did not change the main metabolism profile of [^{18}F]**5**. The decreased rate of [^{18}F]**5** reduced the uptake of [^{18}F]F^- in the bone of mice, and increased slightly the percentage of specific binding to PBR accounting for the total binding as reflected in the autoradiogram of the rat brain. However, the PET image of [^{18}F]**5** for the monkey brain was not improved in comparison with [^{18}F]**2**, which was disturbed by [^{18}F]F^- accumulating into the skull. The significant difference of radioactivity distribution in the bones of mice or rats and monkeys may reflect the species difference between rodents and primates. Therefore, unlike [^{11}C]**1** and [^{18}F]**3**, [^{18}F]**5** may be not a useful PET radioligand, even though it entered the brain and had some specific binding with PBR in the brain. The high accumulation of [^{18}F]F^- in the bone should preclude the in vivo usefulness of [^{18}F]**5** for determining PBR binding in the primate brain. Moreover, the uptake of [^{18}F]F^- should decrease the effective signal of PET image and the accuracy of data if this ligand was employed to quantitatively measure the PBR density in the brain.

3. Conclusion

In this study, the deuterium-substituted [^{18}F]**5** for PBR was designed, synthesized, and evaluated. Ligand [^{18}F]**5** was synthesized by the alkylation of the desmethyl precursor **7** with [^{18}F]**9** in reproducible radiochemical yields. Compared with the non-deuterated [^{18}F]**2**, [^{18}F]**5** displayed a slower metabolic rate in the brain of mice, a lower uptake into the mouse bone, and higher specific binding to PBR in the rat brain with a similar binding affinity for PBR. However, the deuterium substitution did not decrease the radioactivity level of [^{18}F]**5** in the monkey skull due to its remarkable in vivo defluorination, suggesting species difference between rodents and primates. Although [^{18}F]**5** was not be used for the in vivo investigation of PBR in the primates, our results indicated that isotope effect is an effective tool for improving in vivo behaviors of a parent radioligand.

4. Experimental

4.1. General

^{1}H NMR spectra were recorded on a JNM-GX-270 spectrometer (JEOL, Tokyo) with tetramethylsilane as an internal standard. All chemical shifts (δ) were reported in parts per million (ppm) downfield from the standard. FAB-MS were obtained on a JEOL NMS-SX102 spectrometer (JEOL, Tokyo). Column chromatography was performed on Merck Kieselgel gel 60 F_{254} (70–230 mesh). 18-Fluorine (^{18}F) was produced by ^{18}O(p,n)^{18}F nuclear reaction using a CYPRIS HM-18 cyclotron (Sumitomo Heavy Industry, Tokyo). If not otherwise stated, radioactivity was measured with an IGC-3R Curiemeter (Aloka, Tokyo). HPLC was performed using a JASCO HPLC system (JASCO, Tokyo): effluent radioactivity was monitored using a NaI (Tl) scintillation detector system. All chemical reagents with the highest grade commercially available were purchased from Aldrich Chem. (Milwaukee) and Wako Pure Chem. Ind. (Osaka). The animal experiments were performed according to the recommendations of the committee for the care and use of laboratory animals, National Institute of Radiological Sciences (NIRS).

4.2. Chemical synthesis

4.2.1. *N*-(5-Fluoro-2-phenoxyphenyl)-*N*-(2-iodomethoxy-d_2-5-methoxybenzyl)acetamide (8). A mixture of *N*-(5-fluoro-2-phenoxyphenyl)-*N*-(2-hydroxy-5-methoxybenzyl)acetamide[19] (**7**, 38 mg, 0.10 mmol), CD_2I_2 (**6**, 32 μL, 0.40 mmol), and NaH (8 mg, 0.34 mmol) in DMF (2 mL) was stirred at 25 °C for 3 h. The reaction was stopped with AcOEt, and rinsed with water and saturated NaCl solution. After the organic layer was dried over Na_2SO_4, the solvent was removed to give a residue. Column chromatograph of the residue on silica gel with $CHCl_3$/hexane (1/20) gave **8** (8.0 mg, 15%) as a colorless oil; ^{1}H NMR (300 MHz, $CDCl_3$) δ: 7.18–7.40 (2H, m), 6.15–7.33 (9H, m), 4.71 (dd, $J = 7$, 46 Hz), 3.78 (3H, s), 2.20 (3H, s); FABMS (*m/z*): 524.1 (M^++1); Anal. ($C_{23}H_{19}D_2FINO_4$) C, H, N.

4.2.2. *N*-(5-Fluoro-2-phenoxyphenyl)-*N*-(2-fluoromethoxy-d_2-5-methoxybenzyl)acetamide (5). A mixture of **8** (16 mg, 0.03 mmol) and tetrabutylammonium fluoride (1.0 M solution in THF, 2.0 mL) was heated at reflux for 8 h. After THF was removed, the reaction mixture was re-dissolved in AcOEt, and rinsed with water and saturated NaCl solution. After the organic layer was dried over Na_2SO_4, the solvent was removed to give a residue. Column chromatograph of the residue on silica gel with $CHCl_3$/hexane (1/20) gave **5** (10 mg, 70%) as a colorless oil; ^{1}H NMR (300 MHz, $CDCl_3$) δ: 7.38–7.49 (2H, m), 6.71–7.13 (8H, m), 6.28–6.44 (1H, m), 4.75 (2H, dd, $J = 7$, 46 Hz), 3.71 (3H, s), 2.12 (3H, s); FABMS (*m/z*): 416.3 (M^++1); Anal. ($C_{23}H_{19}D_2F_2NO_4$) C, H, N.

4.3. Radiosynthesis

4.3.1. [^{18}F]Fluoride ([^{18}F]F^-). [^{18}F]F^- was produced by the ^{18}O(p,n) ^{18}F reaction on 10–20 atom% $H_2{}^{18}O$ using 18 MeV protons (14.2 MeV on target) from the cyclotron and separated from [^{18}O]H_2O using Dowex 1-X8 anion exchange resin in an irradiating room. The produced [^{18}F]F^- was released from the resin with aqueous K_2CO_3 (3.3 mg/0.3 mL) into a vial containing CH_3CN (1.5 mL)/Kryptofix 222 (25 mg) and transferred into a reaction vessel set in a hot cell.

4.3.2. *N*-(5-Fluoro-2-phenoxyphenyl)-*N*-(2-[^{18}F]fluoromethoxy-d_2-5-methoxybenzyl)acetamide ([^{18}F]5). After [^{18}F]F^- in the reaction vessel was dried to remove H_2O and CH_3CN at 120 °C for 20 min, **6** (200 μL) in *o*-dichlorobenzene (200 μL) was added into the radioactive mixture. Under a He flow (50 mL/min), the resulted [^{18}F]FCD_2I ([^{18}F]**9**) was immediately distilled at 110 °C for 2 min and bubbled in another reactor containing **7** (1.5 mg) and NaH (10 μL, 1.5 g/20 mL DMF) in anhydrous DMF (300 μL) at −15 °C. After maximum radioactivity was trapped into the solution, the reaction was

terminated by adding CH_3CN/H_2O (6/4, 500 μL) and the reaction mixture was applied to a semi-preparative HPLC system. HPLC purification was performed on YMC J'sphere ODS-H80 column (10 mm ID × 250 mm) using a mobile phase of CH_3CN/H_2O (60/40) at a flow rate of 6.0 mL/min. The retention time (t_R) for [^{18}F]**5** was 12.8 min, while that for **7** was 6.7 min. The radioactive fraction corresponding to [^{18}F]**5** was collected in a sterile flask containing polysorbate (80) (75 μL) and ethanol (150 μL), evaporated to dryness under vacuum, redissolved in sterile normal saline (7 mL) and passed through a 0.22 μm Millipore filter to obtain the final product. At the end of synthesis, 100–180 MBq ($n = 4$) of [^{18}F]**5** was obtained as an i.v. injectable solution at a beam current of 10–15 μA and 20–25 min proton bombardment.

4.4. Radiochemical purity and specific activity determinations

Radiochemical purity was assayed by analytical HPLC (column: CAPCELL PAK C_{18}, 4.6 mm ID × 250 mm, UV at 254 nm; mobile phase: $CH_3CN/H_2O = 6/4$). The t_R for [^{18}F]**5** was 6.1 min at a flow rate of 2.0 mL/min. The specific activity of [^{18}F]**5** was calculated by comparing the assayed radioactivity (GBq) with the mass measured from a calibration curve obtained by the carrier UV peaks at 254 nm corresponding to five known concentrations.

4.5. In vitro binding assays

Male Sprague–Dawley rats ($n = 3$) weighing 220–250 g were sacrificed by decapitation under ether anesthesia, and their brains were quickly removed and frozen on powdered dry ice. Brain sagittal sections (20 μm) were cut on a cryostat microtome (HM560, Leica, Bensheim) and thaw-mounted on glass slides (Matsunami Glass Ind., Tokyo), which were then dried at 25 °C and stored at −18 °C until used for experiments. The brain sections were pre-incubated at 25 °C for 20 min in 50 mM Tris–HCl (pH 7.4) buffer. After pre-incubation, these sections were incubated at 37 °C for 30 min in assay buffer containing [^{11}C]**1** (about 1 nM, specific activity: 100 GBq/μmol) or [^{11}C]flumazenil (about 1 nM, specific activity: 190 GBq/μmol). To determine the IC_{50} values of **5** and **8** for the [^{11}C]**1** (for PBR) or [^{11}C]flumazenil (for CBR) binding, the brain sections were incubated with [^{11}C]**1** or [^{11}C]flumazenil using **5** and **8** at nine different concentrations (0.1–1000 nM), respectively. Ten micrometers of **1** or flumazenil was used to determine the nonspecific binding for PBR or CBR in the brains. After incubation, the brain sections were washed three times for 2 min each time with cold assay buffer, dipped into cold distilled water for 10 s, and dried with a warm air flow (about 50 °C). These sections were then placed in contact with imaging plates (BAS-SR 127, Fuji Photo Film, Tokyo) for 60 min to analyze their radioactivity distribution with a FUJIX BAS 1800 bioimaging analyzer (Fuji). Region of interest (ROI) in the sections was identified in the cerebellum. PSL data corresponding to radioactivity in the cerebellum in the presence and absence of the displacement **5** and **8** were determined, respectively. The specific binding for PBR or CBR was defined as total binding minus nonspecific binding of [^{11}C]**1** or [^{11}C]flumazenil. PSL data corresponding to specific binding at each compound concentration were calculated as a percentage in relation to the control specific binding, and were converted to probit values to determine the IC_{50} of each compound.

4.6. Metabolite analysis for mouse plasma and brain tissue

After i.v. injection of [^{18}F]**5** or [^{18}F]**2** (5–10 MBq/100 μL) into ddy mice ($n = 3$), these mice were sacrificed by cervical dislocation at 5, 15, 30, 60 or 120 min. Blood (0.7–1.0 mL) and whole brain samples were removed quickly, respectively. The blood sample was centrifuged at 15,000 rpm (3615 Model, Kubota, Tokyo) for 2 min at 4 °C to separate plasma, which (250 μL) was collected in a test tube containing CH_3CN (500 μL) and **5** or **2** (10 μL, 1.5 mg/5.0 mL of CH_3CN). After the tube was vortexed, for 15 s and centrifuged at 15,000 rpm for 2 min for deproteinization, the supernatant was collected. The extraction efficiency of radioactivity into the CH_3CN supernatant ranged from 70–92% of the total radioactivity in the plasma. On the other hand, the cerebellum and forebrain including the olfactory bulb were dissected from the mouse brain and homogenized together in an ice-cooled CH_3CN/H_2O (1/1, 1.0 mL) solution. The homogenate was centrifuged at 15,000 rpm for 2 min at 4 °C and the supernatant was collected. The recovery percentage of radioactivity into the supernatant was 74–90% of the total radioactivity in the brain homogenate.

An aliquot of the supernatant (100–500 μL) obtained from the plasma or brain homogenate was injected into the HPLC with a highly sensitive detector[25] for radioactivity, and analyzed under the same HPLC conditions described above except the mobile phase of CH_3CN/H_2O with a ratio of 1/1. The percent ratio of [^{18}F]ligand to the total radioactivity (corrected for decay) on the HPLC chromatogram was calculated as % = (peak area for [^{18}F]ligand/total radioactive peak area) × 100.

4.7. Biodistribution in mice

A saline solution of [^{18}F]**5** or [^{18}F]**2** (average of 8 MBq/200 μL, specific activity: 55 GBq/μmol) was injected into ddy mice (30–40 g, 9 weeks, male; $n = 3$) through the tail vein. Three mice for each time point were sacrificed by cervical dislocation at 5, 15, 30, 60, and 120 min after injection, respectively. The whole brain, bone and blood samples were quickly removed and weighed. The radioactivity present in the various tissues were measured in a Packard autogamma scintillation counter, and expressed as a percentage of the injected dose per gram of wet tissue (% ID/g). All radioactivity measurements were corrected for decay.

4.8. Ex vivo autoradiography

A saline solution of [^{18}F]**5** (20 MBq/200 μL, specific activity: 65 GBq/μmol) or a mixture of [^{18}F]**5**

(25 MBq/200 μL) and **1** (1 mg/kg, 200 μL) was injected into a male Sprague–Dawley rat (220–250 g, 9 weeks, male) through the tail vein. At 30 min after injection, the rat was sacrificed by decapitation under ether anesthesia, and the brain was quickly removed and frozen on powdered dry ice. Brain sagittal sections (20 μm) were cut on a cryostat microtome (HM560) and thaw-mounted on glass slides (Matsunami Glass Ind., Tokyo), dried with warm air flow (about 50 °C). These sections were then placed in contact with imaging plates (BAS-SR 127) for 60 min to analyze the radioactivity distribution with the FUJIX BAS bioimaging analyzer (Fuji).

4.9. Monkey PET

PET scan was performed using a high-resolution SHR-7700 PET camera (Hamamatsu Photonics, Hamamatsu) designed for laboratory animals, which provides 31 transaxial slices 3.6 mm (center-to-center) apart and a 33.1 cm field of view. A male rhesus monkey (*Macaca mulatta*) weighing about 5 kg was repeatedly anesthetized with ketamine (Ketalar®, 10 mg/kg/h, i.m.) every hour throughout the session. After a transmission scan for attenuation correction for 1 h using 74 MBq ^{68}Ge–^{68}Ga source, a dynamic emission scan in 3D acquisition mode was performed for 180 min (2 min × 5 scans, 4 min × 10 scans, 10 min × 4 scans). All emission scan images were obtained by treatment using an image analysis software.[28,29] A saline of [^{18}F]5 (80 MBq) was injected i.v. into the monkey, and time-sequential tomographic scanning was performed on a transverse section of the brain for 180 min.

Acknowledgements

The authors are grateful to Taisho Pharmaceutical Co., Ltd for giving us the samples (DAA1106: **1** and precursor: **7**) and helpful suggestions. We also thank the staff of the Cyclotron Operation Section, Radiopharmaceutical Chemistry Section and Brain Imaging Project of National Institute of Radiological Sciences (NIRS) for their support in the operation cyclotron operation, radioisotope production and PET experiment.

References and notes

1. Braestrop, C.; Squires, R. F. *Proc. Natl. Acad. Sci. U.S.A* **1977**, *74*, 1839.
2. Papadopoulos, V.; Amri, H.; Li, H.; Yao, Z.; Brown, R. C.; Vidic, B.; Culty, M. Structure, function and regulation of the mitochondrial peripheral-type benzodiazepine receptor. *J. Pharmacol. Exp. Ther.* **2001**, *299*, 793–800.
3. Diorio, D.; Welner, S.; Butterworth, R.; Meaney, M.; Suranyl-Cadotte, R. *Neurobiol. Aging* **1991**, *12*, 255.
4. Banati, R. B.; Newcombe, J.; Gunn, R. N.; Cagnin, A.; Turkheimer, F.; Heppner, F.; Price, G.; Wegner, F.; Giovannoni, G.; Miller, D. H.; Perkin, G. D.; Smith, T.; Hewson, A. K.; Bydder, G.; Kreutzberg, G. W.; Jones, T.; Cuzner, M. L.; Myers, R. *Brain* **2000**, *123*, 2321.
5. Raghavendra Rao, V. L.; Dogan, A.; Bowen, K. K.; Dempsy, R. J. *Exp. Neurol.* **2000**, *161*, 102.
6. Batra, S.: Iosif, C. S. *Int. J. Oncol.* **1998**. *12*, 1295.
7. Miyazawa, N.; Hamel, E.: Diksic, M. *J. Neurooncol.* **1998**. *38*, 19.
8. Venturini, I.; Zeneroli, M. I.; Corsi, L.; Avallone, R.; Farina, F.; Alho, H.; Baraldi, C.: Ferrarese, C.; Pecora, N.; Frigo, M.; Ardizzone, G.; Arrigio, A.; Pellicci, R.; Baraldi, M. *Life Sci.* **1998**, *63*, 1269.
9. Camsonne, R.; Crouzel, C.; Comar, D.; Maziere, M.; Prenant, C.; Sastre, J.; Moulin, M. A.; Syrota, A. *J. Labelled Comp. Radiopharm.* **1984**, *21*, 985.
10. Pike, V. W.; Halldin, C.; Crouzel, C.; Barre, L.; Nutt, D. J.; Osman, S.; Shah, F.; Turton, D. R.; Waters, S. L. *Nucl. Med. Biol.* **1993**, *20*, 503.
11. Cappelli, A.; Anzini, M.; Vomero, S.; De Benedetti, P. G.; Menziani, M. C.; Giorgi, G.; Manzoni, C. *J. Med. Chem.* **1997**, *40*, 2910.
12. Matarrese, M.; Moresco, R. M.; Cappelli, A.; Anzini, M.; Vomero, S.; Simonelli, P.; Verza, E.; Magni, F.; Sudati, F.; Soloviev, D.; Todde, S.; Carpinelli, A.; Kienle, M. G.; Fazio, F. *J. Med. Chem.* **2001**, *44*, 579.
13. Zhang, M.-R.; Kida, T.; Noguchi, J.; Furutsuka, K.; Maeda, J.; Suhara, T.; Suzuki, K. *Nucl. Med. Biol.* **2003**, *30*, 513.
14. Maeda, J.; Suhara, T.; Zhang, M.-R.; Okauchi, T.; Ichimiya, T.; Inajii, M.; Ohbayashi, S.; Suzuki, K. *Synapse* **2004**, *52*, 283.
15. Pappata, P.; Cornu, Y.; Samson, C.; Prenant, J.; Benavides, B.; Scatton, C.; Crouzel, J. J.; Hauw, A.; Syrota, A. *J. Nucl. Med.* **1991**, *32*, 1608.
16. Cagnin, A.; Brooks, D. J.; Kennedy, A. M.; Gunn, R. N.; Myers, R.; Turkheimer, F. E.; Jones, T.; Banati, R. B. *Lancet* **2001**, *358*, 461.
17. Zhang, M.-R.; Maeda, J.; Furutsuka, K.; Yoshida, Y.; Ogawa, M.; Suhara, T.; Suzuki, K. *Bioorg. Med. Chem. Lett.* **2003**, *13*, 201.
18. Zhang, M.-R.; Maeda, J.; Ogawa, M.; Noguchi, J.; Ito, T.; Yoshida, Y.; Okauchi, T.; Obayashi, S.; Suhara, T.; Suzuki, K. *J. Med. Chem.* **2004**, *47*, 2228.
19. Okubo, T.; Yoshikawa, R.; Chaki, S.; Okuyama, S.; Nakazato, A. *Bioorg. Med. Chem.* **2004**, *12*, 423.
20. Zhang, M.-R.; Ogawa, M.; Furutsuka, T.; Yoshida, Y.; Suzuki, K. *J. Fluoro. Chem.* **2004**, *126*, 1879.
21. Zhang, M.-R.; Tsuchiyama, A.; Haradahira, T.; Yoshida, Y.; Furutsuka, T.; Suzuki, K. *Appl. Radiat. Isot.* **2002**, *57*, 335.
22. Melander, L.; Saunder, W. H., Jr. *Reaction Rates of Isotopic Molecules*; John Wiley & Sons, 1980.
23. Flowler, J. S.; Wang, G. J.; Logan, J.; Xie, S.; Volkow, N. D.; Schlyer, D. J.; Pappas, N.; Alexoff, D. L.; Patlak, C. *J. Nucl. Chem.* **1995**, *36*, 1255.
24. Staley, J. K.; Van Dyck, C. H.; Tan, P.-Z.; Staley, J. K.; Tikriti, M.; Ramsby, Q.; Klump, H.; Ng, C.; Grag, P.; Soufer, R.; Baldwin, R. M.; Innis, R. B. *Nucl. Med. Biol.* **2001**, *28*, 271.
25. Zhang, M.-R.; Haradahira, T.; Maeda, J.; Okauchi, T.; Kawabe, K.; Kida, T.; Obayashi, S.; Suzuki, K.; Suhara, T. *Nucl. Med. Biol.* **2002**, *29*, 469.
26. Takei, M.; Kida, T.; Suzuki, K. *Appl Radiat Isot.* **2001**, *55*, 229.
27. Chaki, S.; Funakoshi, T.; Yoshikawa, R.; Okuyama, S.; Okubo, T.; Nakazato, A.; Nagamine, M.; Tomisawa, K. *Eur. J. Pharmacol.* **1999**, *371*, 197.
28. Okauchi, T.; Suhara, T.; Maeda. J.; Kawabe, K.; Obayashi, S.; Suzuki, K. *Synapse* **2001**, *41*, 87.
29. Maeda, J.; Suhara, T.; Kawabe, K.; Okauchi, T.; Obayashi, S.; Hojo, J.; Suzuki, K. *Synapse* **2003**, *47*, 200.

Psychiatry and Clinical Neurosciences (2004), 58, 531–535

Regular Article

Long-term suppression of methamphetamine-induced c-Fos expression in rat striatum by the injection of c-fos antisense oligodeoxynucleotides absorbed in water-absorbent polymer

JUN'ICHI SEMBA,[1] MAKI WAKUTA[1] AND TETSUYA SUHARA[2]
[1]*Division of Health Sciences, University of the Air and* [2]*Division of Advanced Technology for Medical Imaging, National Institute of Radiological Sciences, Chiba, Japan*

Abstract The use of water-absorbent polymer (WAP) as a hydrogel carrier for the slow delivery of antisense oligodeoxynucleotides (ODN) in the brain, was recently developed. In this experiment, 15-mer phosphorothioate ODN, complementary to c-fos gene absorbed in WAP, was injected in the rat striatum. The expression of c-Fos-immunoreactivity induced by methamphetamine (6 mg/kg, intraperitoneally) around the injection site was suppressed until 5 days after injection. Using this method, it was observed that unilateral injection with c-fos antisense ODN into the rat striatum caused robust ipsilateral rotations after methamphetamine challenge 4 days post injection. This method is simple, and the biological and behavioral effects of antisense ODN in WAP can be maintained for several days even after a single injection into the brain.

Key words antisense oligodeoxynucleotide, c-fos, water-absorbent polymer.

INTRODUCTION

Recently, the intracerebral administration of antisense oligodeoxynucleotides (ODN) complementary to specific mRNA to the brain, was successfully used to prevent the synthesis of target proteins. Since ODN are easily degraded by ribonuclease in the brain, modification of the structure of antisense ODN by phosphorothioate formulations (S-oligo) is usually necessary to maintain their stability. Furthermore, multiple intracerebral injections of antisense ODN over several days[1,2] or continuous infusion by osmotic minipump,[3–5] is usually required to achieve a desired suppression of the targeted protein in a particular brain region. However, these infusion methods are tedious and often cause large tissue damage or require the use of a complicated infusion cannula system to deliver ODN into the brain continuously.[3–5] Recently, Bannai *et al.* developed the hydrogel of water-absorbent polymer (WAP) as a useful carrier for slowly delivering antisense ODN in the brain.[6,7] In the present experiment, we used a single injection of this WAP as a carrier of c-fos antisense ODN, successfully suppressing its expression induced by methamphetamine for 5 days, and inducing ipsiversive rotations after methamphetamine challenge 2 and 4 days after the injection.

METHODS

Male Wistar rats weighing 200–220 g were used. They were housed in groups of 3–4 in a temperature-controlled room under a light/dark cycle (lights on from 7.00 to 19.00 hours) with food and water ad libitum. All animal experiments were carried out under the control of the Guidelines for Animal Experiments at the University of the Air. Under pentobarbital anesthesia, 2 μL of WAP containing 20 μg of ODN to c-fos were injected via a 5-μL Hamilton syringe into the medial striatum (AP = +0.1 mm, L = ±0.24 mm, H = –0.58 mm)[8] over 5 min. For the immunohistochemical study, antisense and sense ODN were injected into the right and left striatum, respectively. For the behavioral study, anti-

Correspondence address: Dr Jun'ichi Semba, Division of Health Sciences, University of the Air, 2-11 Wakaba, Mihama-ku, Chiba 261-8586, Japan. Email: sembaj@u-air.ac.jp

Received 1 December 2003; revised 17 February 2004; accepted 7 March 2004.

sense ODN, sense ODN or saline were injected into the right striatum. The needle was retracted 2 min after the infusion. The 15-mer phosphorothioate oligodeoxynucleotides (ODN) complementary to the c-fos gene, were obtained from Sawady (Tokyo, Japan). The sequences of the antisense and sense ODN were 5′-GAA-CAT-CAT-GGT-CGT-3′ and 5′-ACG-ACC-ATG-ATG-TTC-3′, respectively.[9,10] They were dissolved in saline, and ODN solution was added to WAP (Sanwet IM-1000, Sanyo-Kasei, Tokyo, Japan) to produce an 80-fold gel as indicated by Bannai *et al.*[6,7]

Rats were challenged with intraperitoneal injections of methamphetamine hydrochloride (6 mg/kg) at 1, 3, 5 and 7 days after injection. At 3 h after the methamphetamine challenge, rats were deeply anesthetized with pentobarbital and transcardially perfused with phosphate-buffered saline (PBS), followed by 4% paraformaldehyde and 0.5% picric acid dissolved in PBS. The brains were removed, and after immersion–fixation overnight in the same fixative at 4°C, coronal sections 70-μm thick were prepared on a Vibratome. The immunohistochemical procedures were described previously.[11] The sections were incubated with 10% normal goat serum in PBS for 30 min at 4°C and then with anti-c-Fos rabbit polyclonal antiserum (Santa Cruz, 1 : 4000 dilution) in PBS containing 0.1% Triton X-100 for 12 h at 4°C. They were then rinsed with PBS and incubated with horseradish peroxidase-labeled antirabbit IgG antibody (MBL, 1 : 200 dilution) for 2 h at 4°C. The sections were washed and incubated with 0.5% cobalt acetate in Tris-buffered saline for 10 min. Color reaction by glucose oxidase intensification was carried out by incubating the sections in a solution of 0.04% diaminobenzidine, 0.2% glucose, 0.04% ammonium chloride, and 0.005 U/mL glucose oxidase (Sigma, type V) in PBS at 4°C for 16 h. The sections were rinsed, mounted onto glass slides, dehydrated with graded alcohol and xylene, and coverslipped.

The rotational behavior test was carried out 2 and 4 days after the injection. Systemic methamphetamine (5 mg/kg, sc) was given after a 30-min habituation. The direction in which the rats turned was monitored by video-camera and the total numbers of rotations were counted over a 90-min period.

As shown in Fig. 1, the number of c-Fos-immunoreactive cells was counted in a square region (0.75 mm × 0.75 mm), the dorsomedial corner of which was in contact with the margin of the injection site (L = ± 0.11, H = 0.58 cm) using NIH Image 1.6 software (Wayne Rasband, NIH). At least two slices at three levels (the center [C] of the injection site and +700 μm [A] and −700 μm [P] from the injection site) were taken from each rat. The suppression of c-Fos expression was evaluated from the ratio of the c-fos-immunoreactive cells on the antisense side compared to the sense side.

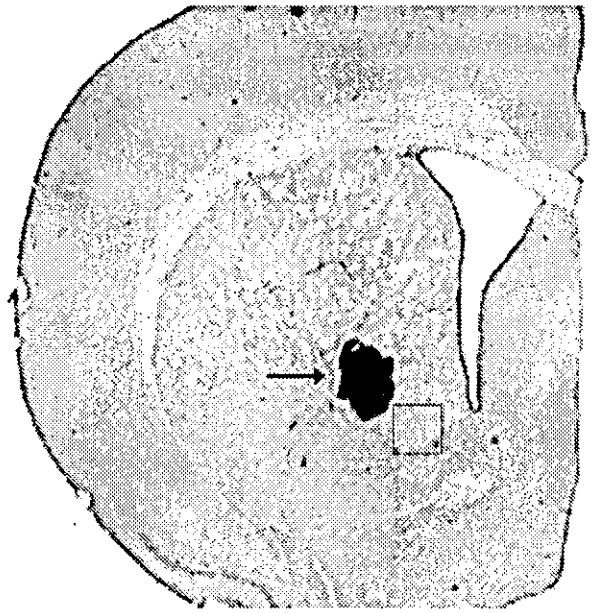

Figure 1. The site of injection of oligodeoxynucleotides and the area where Fos-positive nuclei were counted. The section was stained by Nissl. Fos-IR was counted in the square (0.75 mm × 0.75 mm) in the medial striatum. Arrow indicates the site of oligodeoxynucleotides injection.

RESULTS

Methamphetamine (6 mg/kg) induced robust c-fos-immunoreactivity (IR) in the striatum of naïve rats (data not shown). However, as shown in Fig. 2, intrastriatal infusion of antisense ODN resulted in a significant suppression of c-Fos-IR, while many c-fos-immunoreactive nuclei were stained in the anatomically corresponding area of the striatum injected with the c-fos sense ODN. This finding was in agreement with other experiments in which the same antisense ODN for c-fos were used.[9,10] In a preliminary experiment, we assessed the non-specific effect of sense ODN on the expression of c-Fos-IR. The infusion of sense ODN did not show a significant suppression of c-fos-IR in the striatum after methamphetamine challenge. As shown in Fig. 3 the greatest suppression was observed at the center and anterior, except posterior, sections. This suppressive effect of the antisense ODN was retained until 5 days after the infusion but then diminished at 7 days.

As shown in Fig. 4, unilateral injection of c-fos antisense ODN into the striatum generated methamphet-

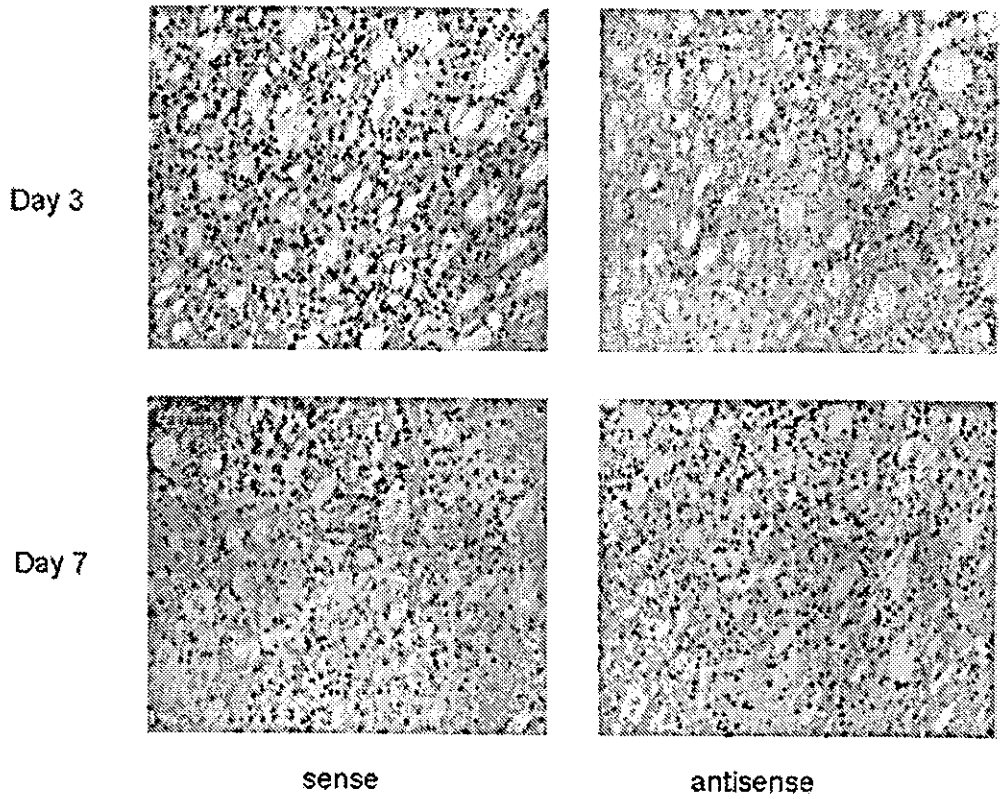

Figure 2. Representative photomicrographs showing Fos-immunoreactive neurons in the medial striatum at a level of the center of the injection site.

amine-induced turning toward the antisense injection side of the brain (ipsiversive). Although, on day 2, control rats injected with saline rotated in both directions and showed no significant rotational bias, the antisense-injected rats rotated more in the ipsiversive than the contraversive direction. On day 4, antisense-injected rats significantly increased ipsiversive rotations compared to those in sense- or saline-injected rats, showing remarkable rotational bias.

DISCUSSION

The present study demonstrated that antisense ODN for c-fos incorporated in WAP, efficiently suppressed the methamphetamine-induced expression of c-Fos protein around the site of the injection for 5 days post injection. Antisense ODN to c-fos were injected into the medial striatum because that is where the highest level of c-Fos-IR occurs, as already reported by other investigators.[12,13] Since Fos protein is rapidly induced by amphetamine and its half-life is relatively short,[14] we can monitor the time course of the effect of antisense ODN absorbed in WAP on the translation of c-fos mRNA. Many investigators have reported that the biological effect of a single injection of c-fos antisense ODN is limited to a time point of no more than 24 h.[9,10,14,15] However, our method can achieve the long-lasting suppression of c-Fos-IR by a single injection of antisense ODN absorbed in WAP.

According to the original method developed by Bannai *et al.*,[7] antisense ODN have been shown to diffuse approximately 800 μm from the edge of the area where WAP was located. The distribution of antisense ODN was compatible with our study where the suppression of c-Fos-IR was observed in the slice 700 μm anterior from the injection site. The reason for the minor suppressive effect of c-Fos-IR in the posterior slice, however, cannot be easily explained. The diffusion of ODN in the posterior direction may be limited, or the robust expression of c-Fos-IR in this region (middle of striatum) may mask the suppressive effect of antisense ODN.

Previous experiments[9,10,16] showed that unilateral injection of c-fos antisense into the striatum generates amphetamine-induced turning toward the antisense injection side of the brain. We also confirmed this

behavioral effect using antisense ODN in WAP. In our experiment, the ipsiversive rotations after methamphetamine challenge were observed even 4 days post injection. This finding also supports the long-term behavioral effect of antisense ODN absorbed in WAP on methamphetamine-induced rotation.

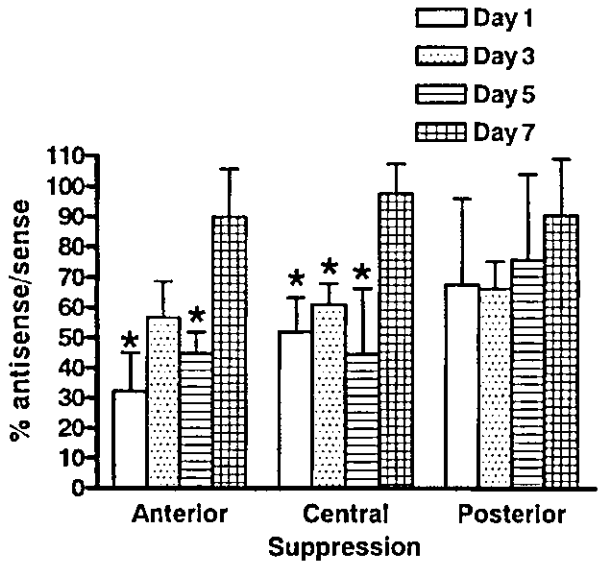

Figure 3. Quantitative analysis of Fos-immunoreactive nuclei in medial striatum following infusion with antisense and sense oligodeoxynucleotides. Values were percentage ratio of c-fos-IR - positive cells on antisense site compared to sense site and were expressed as mean ± SEM ($n = 4$-5). *Significantly different from day 7 ($P < 0.05$) by ANOVA followed by Fisher's Protected Least Significant Difference test.

One of the drawbacks of our method is that the injected 2 μL of WAP made a sphere with a radius of approximately 1 mm at the injection site, even though WAP is known to be biologically non-toxic.[6] A major advantage of this method of infusion, however, is the ability to maintain the duration of exposure to ODN even after a single injection. This method allows the infusion of antisense ODN into a neonatal rat brain for which multiple injections through an injected cannula are impractical.

ACKNOWLEDGMENTS

The authors wish to thank Ms S. Saya and Ms T. Abe for their technical assistance. This study was partly supported by a Grant-in-Aid for Scientific Research from the Ministry of Education, Culture, Sports, Science and Technology, Japan and a grant from the Smoking Research Foundation, Tokyo.

REFERENCES

1. Neumann I, Kremarik P, Pittman QJ. Acute, sequence-specific effects of oxytocin and vasopressin antisense oligonucleotides on neuronal responses. *Neuroscience* 1995; 69: 997–1003.
2. Silvia CP, King GR, Lee TH, Xue ZY, Caron MG, Ellinwood EH. Intranigral administration of D2 dopamine receptor antisense oligodeoxynucleotides establishes a role for nigrostriatal D2 autoreceptors in the motor actions of cocaine. *Mol. Pharmacol.* 1994; 46: 51–57.
3. Landgraf R, Gerstberger R, Montkowski A *et al.* V1 vasopressin receptor antisense oligodeoxynucleotide into septum reduces vasopressin binding, social discrimination abilities, and anxiety-related behavior in rats. *J. Neurosci.* 1995; 15: 4250–4258.

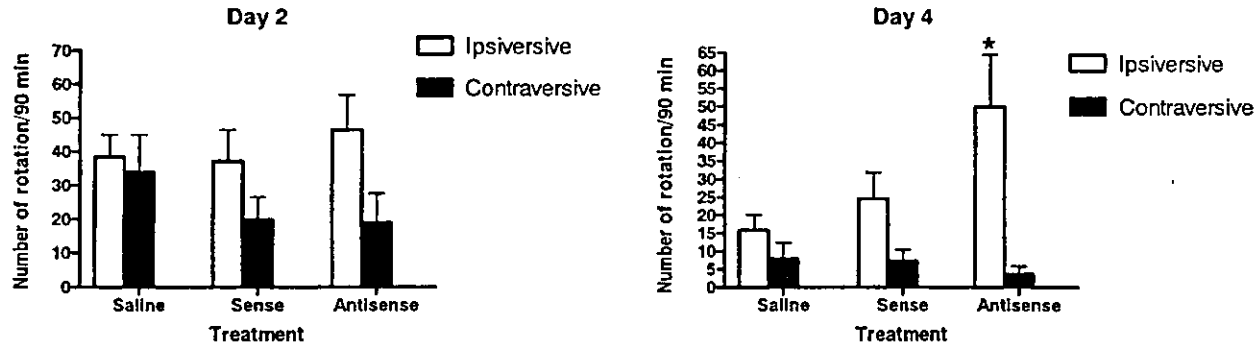

Figure 4. Induction of rotational behavior after methamphetamine treatment in rats injected into the striatum with c-fos antisense oligodeoxynucleotides absorbed in water-absorbent polymer. Rotations in the direction toward the antisense-injected side were termed 'ipsiversive' and those rotating in the opposing direction 'contraversive'. The total numbers of rotations were counted for 90 min after the methamphetamine challenge and were expressed as mean ± SEM ($n = 8$). *Significantly different from 'saline' in ipsiversive rotations ($P < 0.05$) by ANOVA followed by Fisher's Protected Least Significant Difference test.

4. Zhang M, Creese I. Antisense oligodeoxynucleotide reduces brain dopamine D2 receptors: behavioral correlates. *Neurosci. Lett.* 1993; **161**: 223–226.
5. Lu L, Ordway GA. Alpha2C-adrenoceptors mediate inhibition of forskolin-stimulated cAMP production in rat striatum. *Brain Res. Mol. Brain Res.* 1997; **52**: 228–234.
6. Bannai M, Ichikawa M, Nishimura F, Nishihara M, Takahashi M. Water-absorbent polymer as a carrier for a discrete deposit of antisense oligodeoxynucleotides in the central nervous system. *Brain Res. Protoc.* 1998; **3**: 83–87.
7. Bannai M, Ichikawa M, Nishihara M, Takahashi M. Effect of injection of antisense oligodeoxynucleotides of GAD isozymes into rat ventromedial hypothalamus on food intake and locomotor activity. *Brain Res.* 1998; **784**: 305–315.
8. Paxinos G, Watson C. *The Rat Brain in Stereotaxic Coordinates*. Academic Press, San Diego, 1998.
9. Sommer W, Bjelke B, Ganten D, Fuxe K. Antisense oligonucleotide to c-fos induces ipsilateral rotational behaviour to d-amphetamine. *Neuroreport* 1993; **5**: 277–280.
10. Hooper ML, Chiasson BJ, Robertson HA. Infusion into the brain of an antisense oligonucleotide to the immediate-early gene c-fos suppresses production of fos and produces a behavioral effect. *Neuroscience* 1994; **63**: 917–924.
11. Hattori K, Yagi T, Maekawa M, Sato T, Yuasa S. N-Methyl-D-aspartate-induced c-Fos expression is enhanced in the forebrain structures related to emotion in Fyn-deficient mice. *Brain Res.* 2001; **905**: 188–198.
12. Cenci MA, Kalen P, Mandel RJ, Wictorin K, Bjorklund A. Dopaminergic transplants normalize amphetamine- and apomorphine-induced Fos expression in the 6-hydroxydopamine-lesioned striatum. *Neuroscience* 1992; **46**: 943–957.
13. Yoshida H, Ohno M, Watanabe S. Roles of dopamine D1 receptors in striatal fos protein induction associated with methamphetamine behavioral sensitization in rats. *Brain Res. Bull.* 1995; **38**: 393–397.
14. Grzanna R, Dubin JR, Dent GW *et al.* Intrastriatal and intraventricular injections of oligodeoxynucleotides in the rat brain: tissue penetration, intracellular distribution and c-fos antisense effects. *Mol. Brain Res.* 1998; **63**: 35–52.
15. Chiasson BJ, Hooper ML, Murphy PR, Robertson HA. Antisense oligonucleotide eliminates in vivo expression of c-fos in mammalian brain. *Eur. J. Pharmacol.* 1992; **227**: 451–453.
16. Dragunow M, Lawlor P, Chiasson B, Robertson H. C-fos antisense generates apomorphine and amphetamine-induced rotation. *Neuroreport* 1993; **5**: 305–306.

Available online at www.sciencedirect.com
SCIENCE DIRECT
Molecular Brain Research 124 (2004) 88–95
MOLECULAR BRAIN RESEARCH
www.elsevier.com/locate/molbrainres

Research report

Alterations in the expressions of mRNA for GDNF and its receptors in the ventral midbrain of rats exposed to subchronic phencyclidine

Jun'ichi Semba[a,b,*], Nozomi Akanuma[c], Maki Wakuta[a], Noriko Tanaka[a], Tetsuya Suhara[b,d]

[a] *Division of Health Sciences, University of the Air, 2-11 Wakaba, Mihama, Chiba 261-8586, Japan*
[b] *CREST, Japan Science and Technology Corporation (JST), Japan*
[c] *Department of Neuropsychiatry, Faculty of Medicine, Tokyo Medical and Dental University, 5-45 Yushima 1-chome, Bunkyo, Tokyo 151-8586, Japan*
[d] *Division of Advanced Technology for Medical Imaging, National Institute of Radiological Sciences, 9-1 Anagawa 4 chome, Inage, Chiba 261-8555, Japan*

Accepted 15 February 2004

Abstract

Phencyclidine (PCP) produces schizophrenia-like symptoms in normal humans. This suggests that the dysfunction of glutamatergic neurotransmission may play an important role in the pathology of schizophrenia. However, PCP also exerts its effect on the mesolimbic dopamine (DA) system and modulates DA function in the brain, the abnormality of which is proposed to be a main pathology of schizophrenia. Recently, glial cell-line derived neurotrophic factor (GDNF) has been shown to play a protective role for DA neurons against neurotoxic injuries and maintaining DA function in the brain. We hypothesized that subchronic PCP may alter the function of GDNF in the ventral midbrain, where DA cell bodies are localized. Male Wistar rats were injected intraperitoneally with PCP daily for 10 days at 5 or 10 mg/kg, and their brains were removed 24 h after the last injection. The expressions of GDNF and its receptor (GFRα-1 and c-ret) mRNAs in the substantia nigra compacta (SNC) and ventral tegmental area (VTA) were determined by non-radioactive in situ hybridization, and those of GDNF and c-ret mRNA were found to be increased after the PCP subchronic administration. No significant changes, however, were observed in the expressions of GFRα-1 and basic fibroblast growth factor. These results suggest that subchronic PCP may modulate the function of the GDNF system, which exerts a trophic action on DA neurons in the ventral midbrain.

Theme: Development and regeneration
Topic: Neurotrophic factors: expression and regulation

Keywords: c-ret; Dopamine; GFRα-1; Glial cell-line derived neurotrophic factor; In situ hybridization; Phencyclidine

1. Introduction

Phencyclidine (PCP), a non-competitive antagonist of *N*-methyl-D-aspartate (NMDA) receptors, has been shown to produce a schizophrenia-like psychosis with positive and negative symptoms as well as cognitive dysfunction in normal humans [21]. This suggests that the dysfunction of glutamatergic neurotransmission may play an important role in the pathology of schizophrenia. The effect of PCP on brain dopamine (DA) systems has also received special attention [11,22], since alterations in DA functions have been hypothesized in schizophrenia [10]. In particular, DA neurons in the ventral midbrain, which project to the cortical and limbic brain, have been the focus of intensive studies. In animal experiments, repeated exposure to PCP was shown to facilitate DA metabolism in the prefrontal cortex and limbic regions but not in the striatum [11,32]. Although the PCP-induced DA release in the prefrontal cortex may be attributable to the antagonistic action of PCP on NMDA receptors [19], the specific neural circuits that mediate the effect of PCP on the DA system are unknown. It is possible, however, that PCP-induced activation of the mesolimbic DA neurons involves activation of non-NMDA glutamatergic neurotransmission in the ventral tegmental area (VTA) and substantia nigra compacta (SNC) [29], from which DA cell bodies of the nigrostriatal and mesolimbic/mesocortical projections, respectively, originate [5].

Glial cell-line derived neurotrophic factor (GDNF), purified from cultured glial cells, has been shown to selectively

* Corresponding author. Division of Health Sciences, University of the Air, 2-11 Wakaba, Mihama, Chiba 261-8586, Japan. Tel.: +81-43-276-5111x4144; fax: +81-43-298-4379.
E-mail address: sembaj@u-air.ac.jp (J. Semba).

0169-328X/$ - see front matter © 2004 Elsevier B.V. All rights reserved.
doi:10.1016/j.molbrainres.2004.02.011

enhance the survival of midbrain DA neurons [26]. Recent reports showing the protection of DA neurons from neurotoxic injuries [16,25,52] support the notion that GDNF might be a trophic factor for the DA neurons in the ventral midbrain. GDNF signal is mediated by the activation of a multireceptor complex composed of the binding component GFRα-1 and a signaling component, the receptor tyrosine kinase Ret [12,23]. In situ hybridization analysis revealed that GDNF mRNA is expressed in the adult striatum, while most of the DA neurons in SNC express c-ret and GFRα-1 mRNA [33,44,55], suggesting that GDNF may act in a target-derived manner to regulate the survival and metabolic functions of midbrain DA neurons. However, Pochon et al. [39] demonstrated that GDNF mRNA is also highly expressed in DA neurons in SNC and VTA. The colocalization of mRNAs for GDNF and its receptor components in these regions suggests that GDNF also could possess a local presynaptic mode of action on DA cell bodies. However, the issue of whether chronic PCP modifies the function of the GDNF system as a result of altered dopaminergic activity through a blockade of NMDA receptors has still to be clearly delineated. Thus, we investigated the effect of subchronic PCP on the expressions of mRNA for GDNF and its receptors (c-ret and GFRα-1) in the rat midbrain. To allow a comparison with a neurotrophic factor other than GDNF, the expression of basic fibroblast growth factor (bFGF) was determined since it also has a neuroprotective action for DA neurons, although in a manner different from that of GDNF [35].

2. Materials and methods

2.1. Animals

Male Wistar/ST rats weighing 180–200 g were purchased from SLC (Shizuoka, Japan). The animals were housed 3–4/cage in a controlled environment (lights on 07:00 to 19:00, temperature 22 °C) with free access to food and water. All animal experiments were carried out under the control of the Guidelines for Animal Experiments at the University of the Air.

2.2. PCP administration

Rats were injected with 5 or 10 mg/kg of PCP hydrochloride (kindly donated by Yamanouchi Pharmaceuticals, Tsukuba, Japan) intraperitoneally once daily for 10 days. Control rats received saline. Rats were killed by stunning and decapitation 24 h after the final injection. This interval was chosen based on the finding that GDNF mRNA could be upregulated as long as 24 h after various neuronal stimuli [20,46,55].

2.3. Preparation of cRNA probes

Rat GDNF cRNA probe (plasmid generously donated by Dr. M. Saarma, Institute of Biotechnology, University of Helsinki, Finland) consisting of a *Hin*dIII/*Eco*RI fragment corresponding to 9–410 of NM019139 [26] was subcloned into pBluescript SKII (+). Rat GFRα-1 cRNA probe corresponding to 315–866 of U59486 [23] was from the product of RT-PCR with total rat brain RNA, and a *Hin*dIII/*Not*I fragment was subcloned into pBluescript SK (+). Rat c-ret cRNA probe corresponding to 13–292 of U22514+U22513 [7] was from RT-PCR, and a *Hin*dIII/*Not*I fragment was subcloned into pBluescript SK (+). Rat bFGF cRNA probe (plasmid generously donated by Dr. R. Wen, Department of Ophthalmology, University of Pennsylvania) consisting of an *Nco*I/*Xho*I fragment corresponding to 532–1009 of M22427 [49] was subcloned into pBluescript SKM13 (+).

For antisense digoxigenin-labeled RNA probe synthesis, plasmids were linearized using appropriate restriction sites and then transcribed by T3, T7 and SP6 RNA polymerases in the presence of digoxigenin-11-UTP (Roche Diagnostics, Germany). Sense-stranded RNA probes were also generated and used as negative controls.

2.4. Non-radioactive in situ hybridization

Brains were promptly removed, frozen in powdered dry ice and stored at −80 °C. Coronal sections (12 μm thick) were cut using a cryostat, VTA and SNC of the ventral midbrain were selected, and they were studied between antero-posteriority (A/P) −5.2 and −5.3 mm from the bregma [38]. Slices were thaw-mounted on silane-coated slide glasses. The sections were dried on a hot plate at 40 °C and then stored at −80 °C until hybridization.

Non-radioactive in situ hybridization was performed as described previously [47,48]. In order to avoid inter-assay variance, all sections of one brain region from each treat-

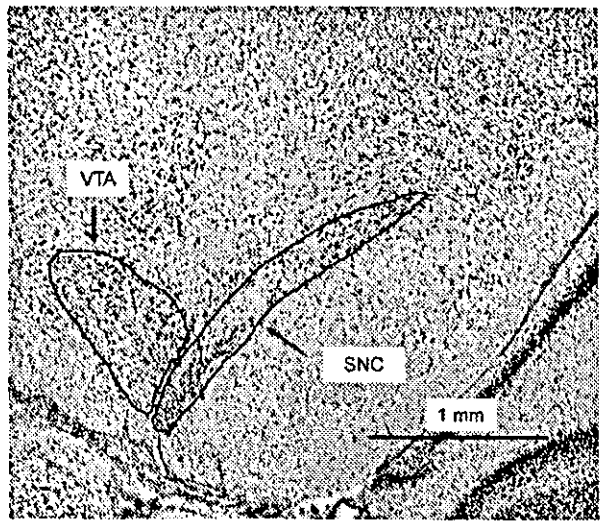

Fig. 1. Determination of sampling areas of VTA and SNC. Figure shows a Nissl stained section corresponding to plates 40–41 (5.2–5.8 mm from bregma) according to the atlas of Paxinos and Watson [38]. Abbreviations: "VTA", ventral tegmental area; "SNC", substantia nigra pars compacta.

ment group were processed together. Sections were post-fixed in 4% paraformaldehyde in 0.1 M phosphate-buffered saline (PBS, pH 7.4) for 20 min at 4 °C. They were then rinsed three times in PBS and acetylated with acetic anhydride. Hybridization was performed with a saturating amount of digoxigenin-11-UTP-labeled cRNA probe (10 μg) diluted in 1 ml of hybridization buffer for 16 h at 52 °C. After hybridization, the slides were washed in 2 × SSC, 50% formamide at 55 °C for 20 min, and treated with 30 μg/ml RNase A for 30 min at 37 °C. They were rinsed in this buffer for 30 min at 37 °C, in 2 × SSC, 50% formamide for 30 min at 55 °C, then in 2 × SSC for 10 min at room temperature, and finally in Tris-buffered saline (TBS, pH 7.4) for 10 min. For immunological detection of digoxige-

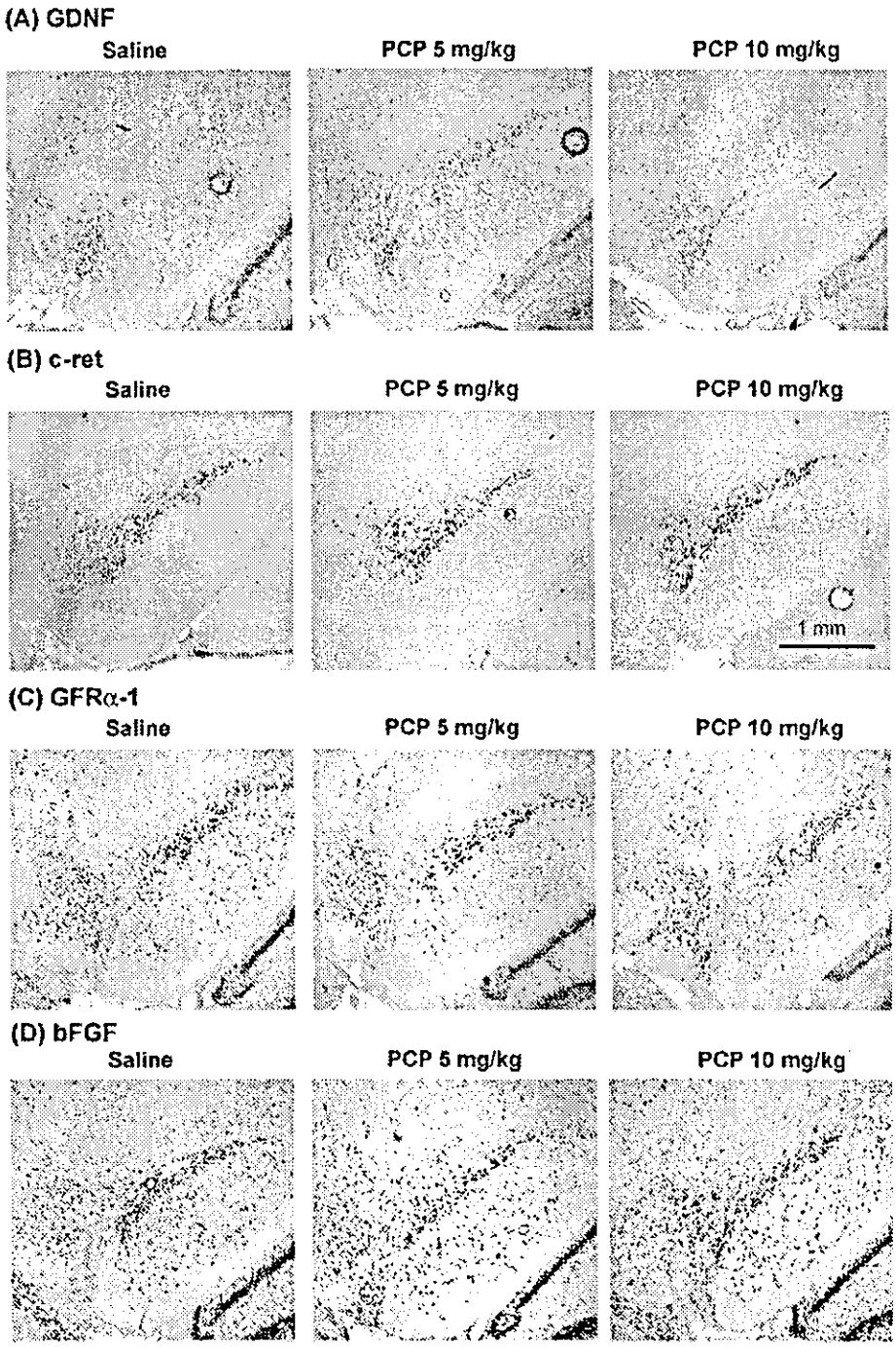

Fig. 2. Representative microphotographs of mRNA-positive cells for GDNF (A), c-ret (B), GFRα-1 (C) and bFGF (D) in SNC and VTA of rats injected with subchronic PCP.

nin, the slides were pre-blocked in 3% bovine serum albumin in TBS for 30 min at room temperature and then incubated with anti-digoxigenin conjugated with alkaline phosphatase (Roche Diagnostics) for 8 h at 4 °C. After incubation, the slides were washed in TBS and developed in a solution of nitroblue tetrazolium and X-phosphate (Roche Diagnostics) in the presence of levamisole (Sigma, USA) for 8 h at room temperature. The color reaction was stopped using 1 mM EDTA in 10 mM Tris–HCl. After a wash in distilled water, the slides were dehydrated and cover-

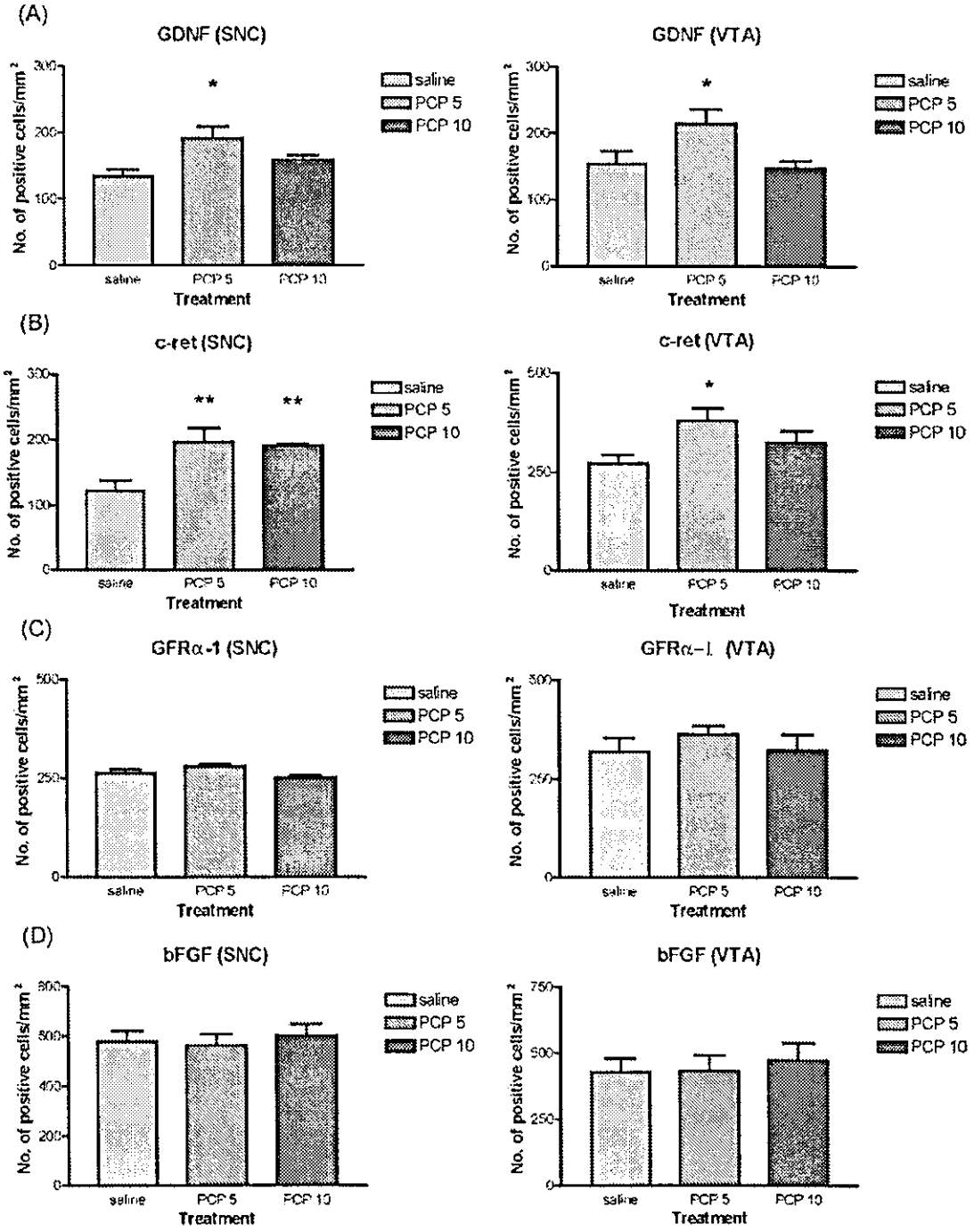

Fig. 3. Effect of subchronic PCP administration on the expression of mRNA for GDNF (A), c-ret (B), GFRα-1 (C) and bFGF (D) in rat SNC and VTA. Animals received daily injections for 10 days and were killed 24 h after the last injection. Results are expressed as mean ± S.E.M. ($N = 8-9$) with post-hoc analysis by Dunnett's test. $^{*}p < 0.05$, $^{**}p < 0.01$ significantly different from control.

slipped. Specificity of the in situ hybridization results was confirmed by the use of sense riboprobes, which showed no detectable signals (data not shown).

2.5. Analysis of hybridization signal

Photomicrographs of rat brain coronal sections depicting the regions of SNC and VTA are shown in Fig. 1. Sampled areas were digitized through a microscope with a CCD camera. Labeled cells in a specified region were counted in at least two sections per animal using a computer-assisted image analysis system equipped with NIH Image 1.6 software (Wayne Rasband, NIH).

2.6. Statistical analysis

The numbers of labeled cells in each region were analyzed by one-way ANOVA. When there was a statistically significant difference ($p<0.05$), Dunnett's post-hoc test was used to compare PCP data with saline control.

3. Results

Although the labeling of GDNF mRNA was modest, non-radioactive in situ hybridization using highly sensitive digoxigenin-labeled cRNA probes enabled us to detect GDNF mRNA-positive neurons in SNC and VTA (Fig. 2(A)) [39]. Subchronic (10 days) treatment with 5 mg/kg of PCP significantly increased the number of GDNF mRNA-positive cells in both SNC and VTA (Fig. 3(A)). A higher dosage (10 mg/kg), however, had no additional effect on the expression level of GDNF. No specific labeling was observed in the substantia nigra reticulata or other regions in the ventral midbrain. As reported previously [6,23,54], high levels of c-ret and GFRα-1 mRNA expressions were detected in SNC and VTA (Fig. 2(B, C)). The mRNA level of GFRα-1, one of the binding components of the GDNF receptor complex, was not influenced by PCP (Fig. 3(C)). However, that of c-ret, the signaling component of the GDNF receptor complex, increased in both SNC and VTA after the subchronic administration of either 5 or 10 mg/kg of PCP (Fig. 3(B)). The structures expressing bFGF mRNA were found to be widely distributed throughout the ventral midbrain (Fig. 2(D)). The number of bFGF mRNA-positive cells, however, was not changed by the subchronic PCP treatment in any of the regions examined (Fig. 3(D)).

4. Discussion

To the best of our knowledge, this is the first report on the effect of chronic PCP on the expression of mRNAs for GDNF and its receptors in rat brain. The major finding of our study was the increased expression of GDNF and c-ret mRNAs in VTA and SNC after daily injections of PCP for 10 days. The GFRα-1 mRNA expression, however, remained unchanged even after chronic administration of a high dose of PCP (10 mg/kg). In a preliminary experiment, the acute injection of 5 or 10 mg/kg PCP did not influence the expression of either GDNF or its receptors within 24 h in any region examined (data not shown). Therefore, the changes in expression of these genes resulted only from repeated administrations of PCP.

We chose a dose of 5 or 10 mg/kg of PCP for our experiments because the striatal DA receptor was reported to be decreased using the same regimen [27,40,42]. In addition, in a preliminary experiment of chronic treatment using more than 20 mg/kg, major weight loss and apparent illness in the animals were noted (data not shown). Thus, a dose of less than 10 mg/kg was thought to have a significant effect on striatal dopamine function without exerting a physical toxic effect.

The effects of pharmacological treatments on the expressions of GDNF and its receptor mRNA in the brain have not been fully investigated. It has been reported that kainate- or pilocarpine-induced seizures increase GDNF mRNA in the hippocampus, striatum and neocortex [20,46,55]. Kainate-induced seizures also increased the expression of c-ret as well as GFRα-1 in the hippocampus [41,55]. Since peripherally administered kainate stimulates kainate receptors and/or releases excitatory amino acid neurotransmitters in the brain, which in turn causes depolarization of neurons, repeated depolarization may be the primary common stimulus causing the induction of GDNF and its receptors in response to seizures [15,20]. Nevertheless, a very prolonged or repeated activation of the neurons may be necessary for an increase in GDNF mRNA, since the acute administration of PCP had no effect in our study, and the dose of pilocarpine needed was high enough to induce status epilepticus in rats [46]. Recently, Chen et al. [8] showed that acute electroconvulsive seizure (ECS) increased GFRα-1 and GFRα-2 mRNA levels in the dentate gyrus of hippocampus, while chronic ECS induced even greater increases. The levels of GDNF and c-ret mRNAs, however, were not significantly changed after either acute or chronic ECS treatment. It is likely that the mechanisms involved in the expression of GDNF receptor genes between pharmacologically and electronically induced seizures are not the same.

In addition to the hippocampal cells, the neuronal activity of DA cells in VTA is also increased by PCP administration [14,37]. Recently, using in vivo microdialysis, Mathe et al. [29] demonstrated that a blockade of NMDA receptors by PCP or MK801 may indirectly lead to a relative hyperfunction of non-NMDA (AMPA and/or kainate) receptors within VTA, despite a reduction of glutamate neurotransmission at NMDA receptors. This finding is also supported by previous microdialysis experiments [19,32], which suggested that PCP facilitates DA release in the medial frontal cortex by

increasing the impulse flow in DA neurons projecting to the cortical area. Electrophysiological studies [9,56] also demonstrated that stimulation of NMDA and/or AMPA receptors alters the activity of DA neurons in VTA, where mRNA for different subtypes of glutamate receptors is expressed [36]. From these experiments, it is assumed that the increased activity of DA neurons in VTA after PCP injection may induce GDNF and c-ret mRNA expressions. Since PCP is less potent in releasing dopamine than kainate, repeated injections of PCP may be needed to increase GDNF mRNA. Increased expressions of mRNA for GDNF and c-ret genes in response to chronic PCP could have beneficial effects on neuronal function and survival. GDNF significantly stimulates dopaminergic sprouting when directly injected into the striatum [43]. The expressions of GDNF and c-ret mRNA in VTA may reflect an autoprotective process in neurons under the neurotoxic effects of PCP. It is also possible that the production of GDNF occurs locally in neurons or glial cells of SNC [45]. The reason for the ineffectiveness of PCP on the GFRα-1 mRNA expression in our study, however, is not known, and this issue awaits further study.

The role of GDNF expression in SNC and VTA is unknown. GDNF is synthesized in striatal cells and retrogradely transported to DA cell bodies in the midbrain [51,53]. Thus, GDNF is known to act as a target-derived trophic agent. Recently, Pochon et al. [39] demonstrated the high expression level of GDNF mRNA in DA cells in SNC and VTA, although the particular characteristics of GDNF-positive cells remained unknown [39]. The localization of GDNF and the two receptor components, GFRα-1 and c-ret, to DA neurons [54] indicates that GDNF also has an autocrine action on these subpopulations of neurons. Our study also suggests that, of the two binding components of the GDNF receptor complex, only c-ret seems to play a crucial role in the regulation of the GDNF signaling pathway in response to chronic PCP, as no change was observed in the expression of GFRα-1 mRNA.

Another possible explanation for the increase of GDNF and c-ret mRNA expressions may be found in chronic PCP-induced apoptosis. It has been demonstrated that the chronic administration of PCP causes neurodegeneration in some brain regions of rats including limbic cortices and hippocampus [13,31,34]. PCP could induce striatal apoptosis via a DA-dependent mechanism, as the drug elevates striatal DA levels [18,32] and DA can be neurotoxic [17,50]. In fact, Mitchell et al. [31] reported that a high dose of PCP could induce apoptotic-like changes in a subpopulation of striatal neurons. However, repeated exposure to PCP has not been reported to induce anatomic damage to DA neurons within the ventral midbrain [13]. The possible apoptotic effect of high doses of PCP may also explain the finding that 5 mg/kg PCP has a greater effect on GDNF and c-ret mRNA than 10 mg/kg.

The possible mechanism by which chronic PCP increased the expression of c-ret mRNA in SNC and VTA can be explained by the alterations of other members of the GDNF family ligands (neurturin, persephin and artemin) and/or receptor components (GFRα-2 and GFRα-3) [1], which function through Ret receptor as the common signal transduction subunit. Lesions of the nigrostriatal DA system by intrastriatal injection of 6-OHDA decrease the c-ret mRNA expression in SNC [3,28], suggesting that the c-ret expression might be related to the loss of DA neurons in SNC. However, to date no pharmacological manipulations that modify the expression of c-ret mRNA have been reported. Furthermore, in SNC and VTA the GFRα-2, 3 mRNA expressions are relatively low compared to that of GFRα-1 mRNA [6,24]. Other GDNF family ligands besides GDNF and other receptor components besides GFRα-1 must be investigated.

We failed to find a significant change in bFGF mRNA expression in any of the regions examined. bFGF is a neurotrophic molecule that has a critical role in the maturation and survival of a variety of neurons [4], and it also has neuroprotective activity over a wide range of neurons [2,35]. However, bFGF has not been shown to influence dopaminergic sprouting [30], whereas GDNF significantly stimulates dopaminergic sprouting when directly injected into the striatum [43]. The different neuroprotective effects of GDNF and bFGF on DA neurons may explain the ineffectiveness of chronic PCP on bFGF mRNA expression.

Finally, we cannot exclude the possibility that unknown transcription factors might mediate the induction of GDNF and its receptors in response to chronic PCP, although the promoter regions of the genes for GDNF and its receptors have not been fully characterized. Further studies will be needed to demonstrate whether chronic PCP might regulate the transcription of these genes.

Acknowledgements

We wish to thank Ms. T. Makino, Mr. H. Takada and Ms. M. Genra for their technical assistance. This study was partly supported by a Grant-in-Aid for Scientific Research from the Ministry of Education, Science, Sports and Culture, Japan and a grant from the Smoking Research Foundation, Tokyo.

References

[1] M.S. Airaksinen, M. Saarma, The GDNF family: signalling, biological functions and therapeutic value, Nat. Rev., Neurosci. 3 (2002) 383–394.

[2] K.J. Anderson, D. Dam, S. Lee, C.W. Cotman, Basic fibroblast growth factor prevents death of lesioned cholinergic neurons in vivo, Nature 332 (1988) 360–361.

[3] D.M. Araujo, D.C. Hilt, P.J. Miller, D. Wen, S. Jiao, P.A. Lapchak, Ret receptor tyrosine kinase immunoreactivity is altered in glial cell line-derived neurotrophic factor-responsive neurons following lesions of the nigrostriatal and septohippocampal pathways, Neuroscience 80 (1997) 9–16.